Published in final edited form as:
Arch Toxicol. 2014 July ; 88(7): 1391–1417. doi:10.1007/s00204-014-1245-3.

The optical, photothermal, and facile surface chemical properties of gold and silver nanoparticles in biodiagnostics, therapy, and drug delivery

Lauren A. Austin,
Laser Dynamics Laboratory, Department of Chemistry and Biochemistry, Georgia Institute of Technology, 901 Atlantic Dr. NW, Atlanta, GA 30332-0400, USA

Megan A. Mackey,
Laser Dynamics Laboratory, Department of Chemistry and Biochemistry, Georgia Institute of Technology, 901 Atlantic Dr. NW, Atlanta, GA 30332-0400, USA

Erik C. Dreaden, and
Koch Institute for Integrative cancer Research, Department of chemical engineering, Massachusetts Institute of Technology, 500 Main St., Cambridge, MA 02139, USA

Mostafa A. El-Sayed
Laser Dynamics Laboratory, Department of Chemistry and Biochemistry, Georgia Institute of Technology, 901 Atlantic Dr. NW, Atlanta, GA 30332-0400, USA

Mostafa A. El-Sayed: melsayed@gatech.edu

Abstract

Nanotechnology is a rapidly growing area of research in part due to its integration into many biomedical applications. Within nanotechnology, gold and silver nanostructures are some of the most heavily utilized nanomaterial due to their unique optical, photothermal, and facile surface chemical properties. In this review, common colloid synthesis methods and biofunctionalization strategies of gold and silver nanostructures are highlighted. Their unique properties are also discussed in terms of their use in biodiagnostic, imaging, therapeutic, and drug delivery applications. Furthermore, relevant clinical applications utilizing gold and silver nanostructures are also presented. We also provide a table with reviews covering related topics.

Keywords

Silver nanostructures; Gold nanostructures; Localized surface plasmon resonance (LSPR); Surface-enhanced Raman scattering (SERS); Plasmonic photothermal therapy (PPTT); Biofunctionalization

Correspondence to: Mostafa A. El-Sayed, melsayed@gatech.edu.

Introduction

The rapid development of nanotechnology has had an invaluable impact on the biomedical field. Nanoparticles, i.e., materials with overall dimensions between 1 and 100 nm, have been utilized in many biomedical applications as contrast agents and biosensors and in therapeutic delivery (Caro et al. 2010; Dreaden et al. 2012a; Murthy 2007). Their nanometer size makes them biologically relevant as they have the ability to permeate cellular membranes and interact with important biomolecules, such as DNA, proteins, and viruses. Additionally, they exhibit several unique properties that differ greatly from their bulk counterparts.

Noble metal nanostructures, such as gold and silver, have attracted much attention due to their unique photo-thermal, chemical, and optical properties (Table 1) (Jain et al. 2007, 2008). Owing to their nanometer size, they exhibit large surface-to-volume ratios that can be leveraged in therapeutic delivery applications. The surface of gold (AuNPs) and silver (AgNPs) nanostructures is also chemical reactive allowing for facile functionalization with various biological stabilizing agents, biomolecules, and chemotherapeutic agents. Their most distinguishable physical property is their enhanced optical performance (i.e., light scattering and absorption). Their remarkable optical properties originate from their unique interaction with light resulting in the collective coherent oscillation of their free conduction band electrons, or the localized surface plasmon resonance (LSPR). The oscillation of the free electrons decays via two processes: (1) radiative decay resulting in the very strong visible scattering of light and (2) nonradiative decay resulting in the conversion of photon energy into thermal energy (Jain et al. 2008). These two decay mechanisms have been readily utilized in bio-diagnostic and imaging (exploiting radiative SPR decay), and therapeutic (exploiting nonradiative SPR decay) applications. In this review, we will discuss common Au and Ag nanostructure syntheses and biofunctionalization approaches as well as some of their biodiagnostic, therapeutic, and clinical applications.

Synthesis

Gold and silver nanostructures synthesized for biological applications are commonly prepared using the colloidal synthesis method. This approach utilizes a metal precursor, a reducing agent, and a stabilizing agent, and allows for the facile tuning of the size, shape, and optical properties of the nanostructures. Some of the syntheses for gold and silver nanostructures are highlighted below.

Gold nanostructures

Gold nanospheres (AuNSs): One of the most widely used gold nanostructures is spherical gold nanoparticles (AuNSs) as they can be easily synthesized in large quantities with relatively high monodispersity (Fig. 1a). Spherical gold nanoparticles, which were first reported by Faraday in 1857, are generally synthesized using Turkevich's citrate reduction method (Faraday 1857; Turkevich et al. 1951). This method produces spherical particles with diameters ≥10 nm and involves the reduction of aqueous chloroauric acid by sodium citrate. By varying the stoichiometric ratio between gold and the reducing agent, sodium citrate, the size of the spherical nanoparticles can be controlled, with larger ratios leading to

particles with larger diameters (Frens 1973). In this method, citrate not only acts as the reducing agent, but it also stabilizes the particles via electrostatic repulsion. In the event that spherical gold nanoparticles of diameters ≤10 nm are required, the Brust method is generally employed (Brust et al. 1994). Developed in 1994, this method involves a two-phase system where gold ions are reduced by sodium borohydride ($NaBH_4$) at an oil–water interface, and tetraoctylammonium bromide (TOAB) is used as the phase transfer catalyst and stabilizing agent. Due to the relatively weak binding between TOAB and the spherical gold nanoparticles, alkanethiols are introduced to prevent aggregation. Most recently, in 2009, Perrault and chen developed a method complementary to the citrate reduction method to produce highly monodispersed spherical gold nanoparticles with diameters of 50–200 nm (Perrault and chan 2009). In this synthesis, hydroquinone is used to reduce chloroauric acid onto the surface of gold nanoparticle seeds. The addition of sodium citrate was shown to improve particle stability and monodispersity at large diameters.

Gold nanorods (AuNRs): Gold nanorods (AuNRs) are another commonly synthesized gold nanostructure as they are readily used in photothermal and NIR applications (Fig. 1b). There are two general colloidal approaches to gold nanorod synthesis: seed-mediated and seedless growth. The seed-mediated growth method was first described by Murphy et al. in 2001 and further explored by Nikoobakt and El-Sayed in 2003 (Jana et al. 2001a; Nikoobakht and El-Sayed 2003). This method, often referred to as the seed-mediated growth method, requires a solution of small seeds (3–5 nm) produced from the reduction of chloroauric acid by $NaBH_4$ in the presence of cTAB. Once formed, the seeds are introduced into a gold (I) growth solution containing ascorbic acid, silver nitrate ($AgNO_3$), and CTAB. The seeds serve as nucleation sites for Au^+ anisotropic reduction to form gold nanorods with transverse diameters similar to those synthesized by the electrochemical method. While the transverse diameter is relatively constant at 10 nm, the length and in turn the aspect ratio of the nanorod can be adjusted by increasing the concentration of $AgNO_3$. Recently, both Murphy and El-Sayed groups have investigated the synthesis of smaller gold nanorods from the seedless growth method (Ali et al. 2012; Jana et al. 2001b). In this synthesis, the growth solution is kept at an acidic pH via the addition of hydrochloric acid, and $NaBH_4$ is added to simultaneously initiate seed formation and gold nanorod growth. The resulting gold nanorods have dimensions of 28 × 8 nm.

Gold nanocages (AuNCs): As recently as 2005, Xia and coworkers have developed another gold nanostructure that has impacted the field of biomedicine (Chen et al. 2005). Gold nanocages (AuNCs), which have exploitable optical properties along with a hollow interior structure, are synthesized via the galvanic replacement method (Fig. 1c) (Chen et al. 2006; Skrabalak et al. 2008). This method uses silver nanocubes, previously synthesized by the polyol reduction of $AgNO_3$, as the sacrificial template for gold nucleation and growth. The replacement spontaneously occurs because the reduction potential of silver is less than gold, which leads to the oxidization and displacement of silver atoms as gold atoms are reduced onto the nanocube surface. The cage-like structure is formed from voids due to gold reduction occurring in a three-electron process, while the oxidation of silver occurs in a one-electron process (i.e., three silver atoms are replaced by one gold atom). The synthesized gold nanocages have a typical edge length of 40 nm and a wall thickness of 3.5 nm.

Silver nanostructures

Silver nanospheres (AgNSs): Spherical silver nanoparticles (AgNSs) are one of the most commonly synthesized silver nanostructures (Fig. 1d). Although spherical silver nanoparticles can be synthesized using the Turkevich method that was previously described for spherical gold nanoparticles, this method tends to produce large particle diameters (50–100 nm) with broad surface plasmon absorption when using citrate as the reducing and capping agent (Turkevich et al. 1951). In order to obtain smaller spherical nanoparticles (5–20 nm), $NaBH_4$ usually replaces citrate as the reducing agent (Fang 1998). More recently, Suzuki and coworkers described a combined seed and laser technique to produce spherical silver nanospheres with diameters ranging from 10–80 nm (Pyatenko et al. 2007). Silver colloid seeds with an average diameter of 8–10 nm were produced via citrate reduction of silver nitrate and subsequent irradiation by the second harmonic Nd/YAG laser ($\lambda = 532$ nm). The silver seeds were then subjected to either a one-step or multistep synthesis, which involves the addition of the silver seeds to a boiling solution of citrate and $AgNO_3$, to produce larger spherical particles with relatively high monodispersity.

Silver nanocubes (AgNCs): Another frequently utilized silver nanostructure in the biomedical field is the silver nanocube (AgNC) as they exhibit enhanced scattering that can be exploited in biological sensing applications (Fig. 1e). First introduced by Xia and coworkers in 2002, silver nanocubes are synthesized by the polyol method, which involves the reduction of $AgNO_3$ with ethylene glycol and utilizes poly(vinyl pyrrolidone) (PVP) as the capping agent (Sun and Xia 2002). This method is kinetically controlled as maintaining a relatively high final silver nitrate concentration and a relatively low molar ratio between PVP and silver nitrate. This allows for the fast nucleation and growth of silver seeds in addition to preventing the formation of twin defects. The fast nucleation and growth reduce twin defect formation. By varying the silver nitrate concentration and growth time, the size of the nanocubes can be controlled.

Silver nanorods (AgNRs): Silver nanorods (AgNRs) are another silver nanostructure that are heavily utilized due to their enhanced biosensing ability (Fig. 1f). Jana et al. (2001c) described a silver nanorod synthesis that is similar to that reported for gold nanorods and produces silver nanorods with lengths that are much small than that achieved by the electrochemical method. In this synthesis, silver seeds with a diameter of 4 nm are produced from the $NaBH_4$ reduction of $AgNO_3$ in an aqueous citrate solution. Once the seeds are prepared, $AgNO_3$ is reduced by ascorbic acid in a solution containing the silver seeds, the cationic surfactant CTAB, and sodium hydroxide (NaOH). larger aspect ratios are achieved through decreasing the amount of silver seeds present in the nanorod growth solution. When using 4 nm silver seeds, silver nanorods with a length of $\sim$42 nm and an aspect ratio of 3.5 are produced. More recently, Mahmoud et al. (2013) were able to synthesize AgNRs with different aspect ratios by using the polyol reduction method at high temperatures and high stirring speeds. The high temperatures and stirring speeds aided in overcoming the thin layer formed around the nanorod surface that is believed to stop nanorod growth.

Biofunctionalization

One of the most advantageous properties of gold and silver nanostructures in the biomedical field is their surface stability. This affords facile surface functionalization with various biological and organic molecules. The relative ease of nanoparticle surface modification, through noncovalent and covalent interactions, allows for not only the replacement of potentially toxic initial stabilizing agents, such as CTAB, but also allows for specific biological targeting, and their use in biodiagnostic and biosensing applications. Noncovalent modifications occur through electrostatic interactions, hydrophobic entrapment, and van der Walls forces, while covalent modifications utilize direct chemical attachment, linker molecules, or click chemistry.

Noncovalent interactions—Electrostatic interactions have been extensively used to functionalize gold and silver nanoparticles to biomolecules, such as DNA, peptides, and antibodies. This mode of functionalization relies on the attraction between two oppositely charged species: the nanoparticle surface and the biomolecule of interest (Fig. 2). The advantage of this interaction is that the biomolecule is not exposed to harsh chemical modifications that could compromise its native, active form. When using this type of nanoparticle functionalization, it is important to consider the impact of the surrounding medium's ionic strength and pH. In 2001, Rotello and coworkers utilized this interaction to functionalize cationic gold clusters with DNA using the negatively charged phosphate backbone of DNA (McIntosh et al. 2001). The stability of the DNA-functionalized gold clusters was confirmed via UV–Vis spectroscopy and dynamic light scattering (DLS). Our group has also used electrostatic interactions to functionalize AuNPs and AuNRs with anti-EGFR antibodies to selectively target and photothermally destroy cancer cells (Huang et al. 2006a, b, 2007). Electrostatic interactions were also used by Yuan et al. (2012) to immobilize an anti-neurogenin 1 (anti-ngn 1) antibody on DL-mercaptosuccinic acid (MSA) stabilized AgNPs. The interaction was established between the anionic carboxyl groups ($–COO^-$) of the MSA-AgNPs and the cationic amine groups ($–NH_3^+$) of the antibody and enabled the labEl-free detection of the synthetic peptide fragment of ngn 1. Rotello and coworkers further exploited noncovalent interactions to successfully load hydrophobic therapeutics, tamoxifen, and *β*-lapachone, to AuNPs (Kim et al. 2009). The AuNPs were designed such that they mimicked micelle structures (i.e., a hydrophobic interior and a hydrophilic exterior), which allowed for the encapsulation of hydrophobic drugs in the hydrophobic pockets.

Covalent interactions—While noncovalent attachment to the nanoparticle surface has its advantages, covalent interactions generally provide greater stability and reproducibility of molecular functionalization (Fig. 2). Chemisorption, or dative bonding, is commonly used to attach thiol-terminated biomolecules and biopolymers to nanoparticle surfaces through strong metal-S bonds. For example, the bond energy between Au and S is 44 kcal mol^{-1} (Dubois and Nuzzo 1992). This interaction is achieved when the sulfur atom donates a lone pair of electrons to the empty orbitals of gold or silver atoms at an interface (Sapsford et al. 2013). Thiolated biopolymers such as PEG and polyoxazoline (PO*x*) have been anchored to gold nanoparticle surfaces through Au–S bonds to enhance the particle's stability in physiological environments as well as avoid nonspecific binding of serum proteins and

opsonization when introduced into in vivo systems (Amoozgar and Yeo 2012; Wang et al. 2011b). Other biocompatible polymers used for physiological nanoparticle stabilization are PVP, poly(styrene sulfonate) (PSS), and poly(lysine) (PLL). Metal-S bond formation has also been used to adhere oligonucleotides to nanoparticle surfaces. Both Mirkin and Alivisatos independently demonstrated oligonucleotide-functionalized AuNPs in 1996, and this work has since been extended to various biomedical applications such as hepatitis C virus detection, intracellular gene regulation, and mercuric ion detection (Alivisatos et al. 1996; Glynou et al. 2003; Lee et al. 2007; Mirkin et al. 1996; Rosi et al. 2006). Targeting ligands such as arginine–glycine–aspartic acid (RGD) and nuclear localizing signal (NLS) peptides have also been conjugated to gold and silver nanoparticle surfaces through the metal-S bond to promote particle internalization by human oral squamous cell (HSC-3) cells and their subsequent nuclear localization (Austin et al. 2011a; Kang et al. 2010a; Oyelere et al. 2007). Functionalization in this system occurred via cysteine residues located within the peptides and the nanoparticle surface.

Many nanoparticle conjugate systems utilize bifunctionalized linkers to covalently attach therapeutic drugs and biomolecules as this reduces the possibility of undesirable structural changes that may arise from direct interaction. It has been demonstrated that proteins that directly interact with the nanoparticle surface, such as those seen in the protein corona, may undergo conformational changes that alter their biological activity (Lundqvist et al. 2008). Commonly used linkers for biomedical applications include oligoethylene glycol (OEG) and PEG polymers modified with amine ($–NH_3^+$), carboxyl ($–COO^–$), isothiocyanate (–N=C=S), or maleimide ($H_2C_2(CO)_2NH$) functional groups. These functional groups allow for conventional coupling strategies, such as carbodiimide-mediated esterification and amidation (Fig. 2) (Liu et al. 2010b). The linker molecules are also modified to contain thiol or disulfide groups to promote their exchange with capping agents at the nano-particle surface. Prabaharan et al. (2009) demonstrated the successful covalent attachment of doxorubicin (DOX) to a hydrophobic inner layer of a folic acid amphiphilic AuNP via a pH-sensitive hydrazone linkage. Their folate-targeted DOX-conjugated AuNP showed selective uptake and DOX release to breast cancer cells. Ying and coworkers also used covalently attached DOX to AgNPs to create a DNA biosensor (Ting et al. 2009). DOX was bound to amine-functionalized AgNPs using an NHS-PEG-NHS linker. Moreover, tumor-targeting antibodies, such as single-chain variable fragment (ScFv) antibodies, have been conjugated to nanoparticles using heterobifunctional PEG linkers and EDc/NHS coupling (Qian et al. 2008). Click chemistry, most notably azide-alkyne Huisgen cycloaddition, which involves the use of a copper catalyst, has also been utilized for nanoparticle functionalization and related applications (Fischler et al. 2008; Zhu et al. 2012).

Imaging and biodiagnostic applications

As stated previously, noble metal nanostructures offer unique physical and optical properties that can be exploited in in vitro and in vivo imaging and diagnostic applications. Their nanometer size is comparable to many important biological molecules (i.e., DNA, proteins, viruses, etc.) and allows them to penetrate cellular and tumorigenic systems. even more beneficial than size are their optical properties, namely their ability to strongly scatter light and enhance the local electric field (Jain et al. 2007, 2008). These properties, stemming from

surface plasmon resonance, are readily utilized to lower biomarker detection limits, monitor disease progression, and identify diseased systems.

LSPR shift—One of the most unique properties of Au and Ag nanostructures is LSPR. LSPR is the coherent oscillation of the nanostructure's conduction band free electrons in resonance with the incident electromagnetic field. A metallic nanostructure's LSPR is highly dependent on the size, shape, and dielectric constant of the nanostructure as well as the dielectric function of the surrounding medium (Jain et al. 2007, 2008). Due to the sensitivity of a nanostructure's LSPR to its surrounding environment, biosensors based on the shift of the LSPR have been developed (Petryayeva and Krull 2011). There are two general approaches to LSPR sensors: (1) shifts due to nanostructure aggregation and (2) shifts resulting from biomolecule–surface interactions.

The first approach is based on the interparticle plasmon coupling between nanostructures as the interparticle distance changes. Since a nanostructure's electromagnetic field (EM) is localized at the surface and decays exponentially as the distance away from the surface is increased, interparticle coupling is maximized when nanostructures are in an aggregated state (Jain et al. 2006; Petryayeva and Krull 2011). The aggregated state results in a red-shift of the LSPR and is often noticeable to the naked eye via color change of the nanostructure in solution (e.g., gold nanosphere aggregation is indicated by a color change from red to blue). The relationship between the LSPR shift and the interparticle distance is shown in Eq. 1 (Willets and Van Duyne 2007):

$$\Delta\lambda_{\mathrm{LSPR,max}} = m\Delta n\left[1-\exp\left(\frac{-2d}{I_d}\right)\right] \quad (1)$$

where m is the bulk refractive index of the nanostructure [in nm per refractive index unit (RIU)], Δn is the change in the refractive index (in RIU), d is the effective thickness of the absorbant layer (in nm), and I_{d} is the characteristic EM field decay length (in nm).

One of the first reports of using aggregation-based LSPR sensing came from Mirkin et al. (1996) (Elghanian et al. 1997). In this study, two sets of 13 nm AuNPs were functionalized with noncomplementary strands of oligonucleotides via thiol groups. When the two noncomplementary oligonucleotide-AuNPs were introduced into a solution containing complementary ssDNA, the solution's color changed from red to blue indicating the successful hybridization between the ssDNA target and the oligonucleotide-AuNPs. Mirkin and coworkers have further expanded this ssDNA oligonucleotide-AuNP sensor to single-nucleotide base detection and metal ion detection (Fig. 3) (Lee et al. 2007; Storhoff et al. 1998). Aslan et al. (2004) employed aggregation-based LSPR sensing in the detection of glucose using dextran-coated nanogold. In this work, dextran-AuNPs were initially aggregated using concanavalin A (con A), a carbohydrate-binding protein. The addition of glucose, which competitively binds to con A, reduced nanogold aggregation, resulting in a LSPR blue shift as well as a decrease in the plasmon absorbance at the aggregated wavelength (650 nm). Moreover, silver nanoparticle LSPR aggregation assays have been utilized to detect enzyme reactions, such as those involving the consumption of adenosine triphosphate (ATP) (Wei et al. 2008).

The second approach to LSPR shift assays originates from the sensitivity of the LSPR to the refractive index near the nanostructure surface as demonstrated in Eq. 1. As the equation parameters indicate, the use of this assay is for situations in which the absorbant layer is negligible and the analyte of interest is located within the near field of the nanostructure surface (Petryayeva and Krull 2011). To assess assay performance, a sensitivity factor (SF) was used. The SF is defined as the LSPR wavelength shift per unit change in the effective refractive index of the surrounding medium and is expressed in units of nm RUI^{-1}. Our group as well as others has shown that a nanoparticle's SF, due to its dependence on the LSPR, is greatly affected by the shape, size, and metal choice (Haes et al. 2004b; Lee and El-Sayed 2006; Liu and Huang 2013; Sherry et al. 2005). An early investigation, conducted by englebienne, showed the use of the LSPR shift to infer apparent affinity constants between protein antigens and antibodies (Englebienne 1998). The LSPR shift was detected using an automated photometer and produced results that were in good agreement with those determined from traditional methods (i.e., Scatchard plots). Nath et al. later applied this approach in a planar, chip-based format in an attempt to detect biotin–streptavidin binding using a UV-visible spectrophotometer (Nath and Chilkoti 2001). AuNPs that were immobilized on a transparent substrate to allow for UV-visible spectroscopic measurements were functionalized with biotin and incubated with increasing concentrations (e.g., 0.3–100 μg/mL) of streptavidin. A detection limit of ∼1 μg/mL and a dynamic range of ∼1–30 μg/mL were achieved, which demonstrated the analytical sensitivity of this assay. Since these initial “proof of concept” experiments, the LSPR shift principle has been applied to Alzheimer's disease detection (Ag nanotriangles), the simultaneous detection of pathogenic *Escherichia coli* (*E. coli*) and Salmonella tryphimurium (AuNRs with varying aspect ratios), neurotransmitter detection (multiblock Au and Ag NRs, AuNPs), and glucose detection (AgNSs) (Baron et al. 2005; Choi et al. 2013; Haes et al. 2004a; Tashkhourian et al. 2011; Wang and Irudayaraj 2008).

Enhanced Rayleigh scattering—Au and Ag nanostructures exhibit enhanced Rayleigh (elastic) scattering originating from their LSPR. The resulting scattered light is heavily dependent on the nanostructure shape and size, as larger nanostructures and those that contain corners (i.e., cubes, cages, etc.) scatter light more strongly (Jain et al. 2007, 2008). Their enhanced light scattering provides several advantages when used as a biological imaging or sensing agent. The scattered light is much brighter (4–5 orders of magnitude) than the most efficient fluorophores, is much stronger than background sample matrices, is resistant to photobleaching, and does not require expensive strong excitation sources.

Enhanced Rayleigh scattering has been readily used for cellular imaging and utilizes a conventional light microscope equipped with a dark field condenser. The dark field condenser is used to allow only the sample's scattered light, which is at the frequency of the SPR, to be collected by the microscope's objective. In 2005, El-Sayed et al. (2005) demonstrated the great sensitivity of using dark field light scattering to identify cancerous cells. AuNPs were labeled with anti-epidermal growth factor receptor (anti-EGFR) antibodies, which specifically target the EGFR protein on cell membranes. Cancerous cells are known to have significantly higher EGFR protein expression on their cell membrane when compared to healthy cells. Anti-EFGR conjugated AuNPs were incubated with

cancerous and healthy cells and imaged using a dark field microscopy. It was evident from dark field images that the cancerous cells exhibited stronger light scattering resulting from the specific labeling of the anti-EFGF-AuNPs. El-Sayed and coworkers have also used the enhanced light scattering in a dark field arrangement to identify AuNP and AgNP nuclear localization after conjugation with nuclear localizing sequence (NLS) peptides (Fig. 4a) (Austin et al. 2011a; Kang et al. 2010a; Mackey et al. 2013; Oyelere et al. 2007). Austin et al. (2011b) utilized AgNP light scattering to image cancer cell communities during programmed cell death. Human oral squamous cell carcinoma (HSC-3) cells were incubated with increasing concentrations of nuclear-targeted AgNPs, which were previously shown to induce apoptosis. Dark field microscopy was used to image the treated cell communities for ∼24 h and captured nonprofessional phagocytic activity and cellular clustering as a result of nuclear-targeted AgNP incubation. Recently, antibody-functionalized AuNPs that are specific for *E. coli* were used as light scattering reporters to quantify bacteria colonies (Xu et al. 2012). This method provided a detection limit of $\sim 10^4$ CFU/mL and was obtained within 15–30 min.

In addition to cellular imaging, the plasmonically enhanced light scattering can also be used in biomarker or analyte detection. As mentioned previously, the LSPR is strongly affected by changes in the refractive index of the surrounding medium and thus can shift upon changes in molecule–surface interactions. The LSPR is composed of both absorption and scattering components, and therefore, a shift in the LSPR results in a shift of the light scattering wavelength. Since LSPR shift assays were discussed in detail in the above section, other light scattering sensors will be highlighted. Du et al. (2008) utilized the enhanced light scattering of antibody-AuNPs to develop a homogeneous noncompetitive immunoassay that was consistent with traditional enzyme-linked immunosorbent assays (ELISA). The concentration-dependent increase in AuNP light scattering, after the addition of a model analyte, provided a detection limit of 10 ng/mL and allowed for analyte detection in human serum samples. Moreover, dynamic light scattering (DLS) has been coupled with Au nanoprobes to detect important biomolecules, such as free prostate-specific antigen (f-PSA) and target DNA sequences (Dai et al. 2008; Jans et al. 2009; Liu et al. 2008). In the former, Huo and coworkers conjugated capture and detector anti-PSA antibodies to AuNSs and AuNRs, and quantified the amount f-PSA present through the formation of dimers, trimers, and oligomers (Fig. 4b) (Liu et al. 2008). DLS-AuNP coupled biomolecule detection provides many advantages, such as simple sample preparation, a one-step homogenous assay format, and orders of magnitude in sensitivity enhancement.

Surface-enhanced Raman scattering (SERS)—Raman spectroscopy is a spectroscopic technique that provides details about the vibrational modes in a system. This technique is based on the inelastic scattering of photons, usually from monochromatic (i.e., laser) light. The energy difference (i.e., frequency shift) between the incident light and the Raman scattered light is indicative of the energy of a molecular vibration. Raman scattering is a very inefficient process, resulting in a low detection sensitivity that is incompatible with biological samples. In order to overcome weak signals, plasmonic nanostructures, such as Au and Ag, have been utilized in an approach termed SERS. Raman signal enhancement occurs when a molecule is located within the near field of the nanostructure's LSPR

(approximately the nanostructures diameter) and can result in up to 10^{14} enhancement compared to traditional Raman scattering (Nie and emery 1997; Petryayeva and Krull 2011).

Although SERS was first reported in 1973 and the cause of this effect has been heavily studied, the exact mechanism that results in surface enhancement has not been completely elucidated. There are two generally accepted mechanisms, the electromagnetic mechanism and the chemical mechanism (Caro et al. 2010). The electromagnetic mechanism requires the excitation of a nanostructure's LSPR, which leads to an increase in the local EM field surrounding the nanostructure and intensified electronic transitions of molecules located in close proximity to the nanostructure's surface (Schatz et al. 2006). The chemical mechanism involves charge transfer interactions between the nanostructures and the molecules adsorbed onto the nanostructure's surface (Otto and Futamata 2006). Of the two mechanisms, the electromagnetic mechanism is the dominant mode of enhancement.

Like many of the bioanalytical approaches mentioned previously, the use of Au and Ag nanostructures allows for labEl-free SERS detection and molecular fingerprinting. Kneipp et al. (1998) reported the ability of Ag colloids to detect a single DNA base molecule (adenine), having intrinsic Raman scattering at 735 and 1,330 cm^{-1} due to the base's ring-breathing mode. Label-free SERS has also allowed for cancer identification using cancer-targeting AuNRs. In this work, El-Sayed and coworkers incubated anti-EGFR-AuNRs with cancerous and healthy cell lines and recorded the resulting SERS spectra (Huang et al. 2007). SERS spectra obtained from cancerous cells showed highly resolved molecular vibrations characteristic of bound AuNRs, while poorly resolved spectra were seen with healthy cells. More recently, label-free SERS detection has allowed for live cell molecular probing (Austin et al. 2013; Kang et al. 2012; Kneipp et al. 2002, 2006). Kneipp et al. (2002, 2006) were able to obtain SERS spectra of endosomal compartments in live epithelial and macrophage single cells. Their use of unmodified AuNPs resulted in particle aggregation and aided in Raman enhancement. AuNPs have also been utilized to obtain SERS spectra of living HSC-3 cells throughout the entire life cycle (Kang et al. 2012). Since traditional methods for cell cycle analysis utilize DNA content to decipher between phases and the nucleus controls cellular function, AuNPs were functionalized with NLS peptides to promote AuNP nuclear localization. The AuNP confinement to a localized region allowed for low concentrations (0.05 nM) of AuNPs to be used and increased plasmon coupling between nanoparticles. The obtained SERS spectra indicated phase-specific SERS bands and resulted in a dynamic profile of cell cycle progression after release from G1 synchronization. Real-time SERS assessment of cancer cells treated with 100 μM cisplatin or 5-fluorouracil (5-FU) revealed three “SERS death bands” that were used to evaluate drug efficacy (Fig. 5a). The cell viability ratios from the SERS death bands produced were consistent with cytotoxicity measurements obtained from traditional absorbance-based assays (Austin et al. 2013).

SERS Raman reporters, in conjunction with metal nanostructures, have also been heavily utilized in biological applications. Reporters are generally Raman active dyes with a distinct Raman vibrational band that can be detected in complex solution matrices. when reporters are adsorbed or covalently attached to a metal nanostructure, their Raman scattering results from the excitation of the nanostructure's LSPR and does not require an excitation source in

resonance. This allows for multiple targets to be identified at once. SERS multiplex detection was utilized in the simultaneous identification of different DNA and protein molecules as well as deciphering between co-cultured cancer cells (Hsin-Neng and Tuan 2009; Kang et al. 2010b; Lee et al. 2014; Maiti et al. 2011; Sun et al. 2007; Wang et al. 2013). Raman reporters have also been used to detect femtomolar concentrations of PSA. Grubisha et al. (2003) designed a 30 nm AuNP to contain Raman reporter, 5,5′-dithiobis(succinimidyl-2-nitrobenzoate) (DSNB), and anti-PSA antibodies. These functionalized AuNPs were incubated with increasing concentrations of f-PSA and provided a detection limit of 160 fg of f-PSA. Recently, silica-encased 90 nm gold cores functionalized with trans-1,2-bis(4-pyridyl)ethylene (BPE) were able to be detected through bone using a combination of SERS and spatially offset Raman spectroscopy (SORS) (Sharma et al. 2013). Bone thicknesses (3–8 mm), probed in this work, mimicked those seen in the human skull and demonstrated the potential use of this technique to noninvasively probe the brain in vivo. Moreover, Raman reporters have enabled in vivo SERS imaging in other tissues (Keren et al. 2008; Maiti et al. 2012; Zavaleta et al. 2009). Nie and coworkers reported tumor detection in nude mice bearing a human head and neck squamous cell carcinoma (Tu686) xeno-graft tumor (Qian et al. 2008). AuNPs were functionalized with malachite green (Raman reporter), ScFv EGFR antibodies (targeting ligand), and PEG (particle stability) and were found to localize in the tumor site after tail vein injection. AuNPs that did not contain the targeting ligand showed Raman reporter signals in the liver (Fig. 5b). Jokerst et al. (2012) coupled SERS and photoacoustic imaging using AuNRs with an aspect ratio of 3.5 to detect and resect induced ovarian tumors in live mice. SERS imaging allowed for tumor and normal tissue margins to be clearly visualized.

Metal-enhanced fluorescence (MEF)—Although fluorescent labels can suffer from low signal to noise ratios and photobleaching, they are commercially available and therefore are heavily used in biochemical assays. In an effort to circumvent these drawbacks, fluorescent labels are coupled with metal nanostructures in an approach termed metal-enhanced fluorescence (MEF). When a fluorophore is within 1–3 nm from the nanoparticle surface, its fluorescence is quenched due to electron transfer processes. However, if it is within 4–10 nm of the metal surface, its emission is significantly enhanced. The resulting fluorescent enhancement has been attributed to local EM field enhancement near the nanostructure's surface as well as a decrease in the fluorophore's lifetime due to interaction with the nanostructure (Aslan et al. 2005).

Immunoassays and nucleotide sensing are two MEF applications that have been heavily investigated. Geddes and coworkers reported successful RNA sensing via MEF using silver island films (SIF) (Aslan et al. 2006). Target RNA was tagged with TARMA, a fluorescent probe, and annealed to a DNA anchor probe in one step. The fluorescence emission of TARMA was significantly enhanced by the SIF, leading to a lower detection limit of 25 fmol and a signal to noise ratio greater than 20. This detection format, while less sensitive than traditional RNA assays, provides a more cost- and time-effective approach to RNA detection as RNA target amplification is not required. MEF has also been utilized to study supramolecular complexes, such as the ribosome (Bharill et al. 2010; Mandecki et al. 2008).

Nanoparticle surface energy transfer (NSET)—Many biological applications, especially those that probe protein interaction and enzyme activity, utilize Förster resonance energy transfer (FRET). FRET is a well-studied energy transfer mechanism between two fluorescent molecules that are separated by less than 10 nm. Due to their small separation, energy can be passed from one fluorophore (donor) to the other fluorophore (acceptor) through a nonradiative process (Jue 2010). This energy transfer results in an increase in the acceptor's fluorescence emission and a decrease in the donor's fluorescence. The small distance separations (<10 nm) required for energy transfer to occur is a major drawback to FRET. In order to overcome this distance limitation, researchers have employed nanostructures to act as the acceptor. The resulting energy transfer, termed nanoparticle surface energy transfer (NSET), can increase the Förster distance by a factor of ∼2. The FRET interaction between a dye and a metallic nanoparticle is still dipole–dipole in nature, but differs because the nanoparticle has a surface and an isotropic distribution of dipole vectors to accept energy from the donor (Dulkeith et al. 2005; Pustovit and Shahbazyan 2011). Furthermore, the increased quenching ability from the particle is related to its large molar extinction coefficients ($\sim 10^8$ to $\sim 10^9$ $M^{-1}cm^{-1}$ for 15–30 nm AuNPs compared to $\sim 10^5$ $M^{-1}cm^{-1}$ for dyes), which results in a large increase in its transition dipole moment. Additionally, it has been shown experimentally that replacement of an acceptor dye with a metallic nanoparticle changes the distance dependence of the transfer efficiency from $1/R^6$ to $1/R^4$ (Bhowmick et al. 2006; Jennings et al. 2006; Pustovit and Shahbazyan 2011; Swathi and Sebastian 2007; Yun et al. 2005).

One of the most recognizable applications of NSET is the assessment of DNA hybridization as well as cleavage by nucleases. As these are inverse processes, the donor molecule's fluorescence will either be enhanced or quenched depending on the event being studied. These applications have been extensively studied by Ray and coworkers using AuNPs between 15 and 25 nm in diameter (Griffin et al. 2009; Ray et al. 2006, 2007). Recently, NSET has been employed in biomarker detection. Immunosensing of IgG, an immunoglobulin that has been identified as a good marker for various diseases, has been demonstrated by Tao et al. (2014) through the use of gold nanoparticles and FITC-labeled IgG antibodies. In this assay, NSET was controlled through the binding affinity of AuNPs to FITC-anti-IgG antibodies when an immunological response was triggered (i.e., the addition of IgG). when no IgG was present, FITC emission was quenched as the antibodies were in close proximity to the nanoparticle surface. However, when increasing concentrations of IgG were introduced, FITC fluorescence was restored. Fluorescence restoration was linearly proportional to IgG concentrations and provided accurate measurements of IgG concentrations in human serum.

Therapeutic applications

Gold nanostructures

Photothermal therapy: Owing to their characteristic LSPR, AuNPs can absorb light with resonant frequency, but in addition to the strongly enhanced light energy decaying via radiative processes (i.e., scattering), energy can also decay via nonradiative processes. Specifically, the LSPR allows for the coherent oscillation of electrons within the metallic lattice, and these electrons collide (electron–electron relaxation) on a femtosecond

timescale, producing electrons with temperatures up to 1,000 K. The excited electrons then interact with the phonons in the metallic lattice (electron–phonon relaxation) on a picosecond timescale, transferring their energy to the phonons and thus increasing the temperature of the metallic lattice by about 30 °C. The metallic lattice “cools off” via slower phonon–phonon interactions (∼100 ps) and subsequent dissipation of heat to the surrounding medium (El-Sayed 2001; Link and El-Sayed 2003). The ability for these particles to heat the surrounding medium upon excitation, along with the sensitivity of cancer cells to hyperthermia, is exploited in the cancer treatment method of plasmonic photothermal therapy (PPTT) (Huang et al. 2006b; Nolsoe et al. 1993). Plasmonic AuNPs are ideal candidates as photothermal contrast agents. They can be specifically attached to cancer cells via molecular targeting or systemically delivered to tumor sites via the enhanced permeability and retention (EPR) effect (Iyer et al. 2006). Upon accumulation of the AuNPs at the disease site of interest, they can be triggered via external radiation, causing temperature increases characteristic of hyperthermia, and subsequently inducing apoptosis (Bert et al. 2002; Dickerson et al. 2008). Not only can the AuNPs target the disease site of interest for targeted PPTT, but their LSPR is tuned such that the particles can be triggered by near-infrared (NIR) light (650–900 nm) that easily passes through physiological tissue with minimal interference with water and hemoglobin (Weissleder 2001).

The first demonstrations of PPTT were done using spherical AuNPs, which do not have a characteristic LSPR in the NIR region, yet Lin and coworkers were still able to successfully show the destruction of lymphocyte cells after attachment with antibody-conjugated AuNPs and subsequent nanosecond-pulsed visible laser exposure (Pitsillides et al. 2003). El-Sayed and coworkers later employed a similar technique of attaching antibody-conjugated AuNPs to human oral squamous carcinoma cell (HSC-3) cells, only using a continuous wave (cw) visible laser to induce cell death (Huang et al. 2006b).

Since their LSPR can be easily tuned to the NIR frequency, gold nanoshells (silica–gold core–shell NPs) were exploited in PPTT first by Halas and West (Hirsch et al. 2003; O'Neal et al. 2004). These gold nanoshells were simply functionalized for biocompatibility with polyethylene glycol (PEG) and did not exhibit any targeting abilities, other than the specific accumulation in murine colon carcinoma (CT26.WT) tumor tissues by the EPR effect. Upon NIR laser exposure, the photon energy absorbed by the gold nanoshells is essentially translated to thermal energy, so much so that temperature increases of up to 37 °C were recorded intratumorally. This PPTT treatment resulted in complete tumor ablation in tumors specifically bearing the gold nanoshell photothermal contrast agent. El-Sayed and coworkers later demonstrated the use of AuNRs for the NIR-triggered PPTT of HSC-3 tumor cells (Dickerson et al. 2008; Huang et al. 2006a). Initially, they used antibody-conjugated AuNRs for the selective labeling of cancer cells in vitro (Huang et al. 2006a). Upon attachment of these photothermal contrast agents to the cell membrane, NIR laser exposure activated the AuNRs, such that they released enough heat to induce membrane destruction in the labeled cells. The group took this same technique into the in vivo regime, utilizing PEG-AuNRs that were not specific for cellular labeling, but were bio-compatible and able to accumulate in HSc-3 tumor tissue due to the EPR effect (Dickerson et al. 2008). These photothermal contrast agents were systemically delivered to mice, allowed to accumulate in tumor tissue, and then selectively activated via NIR laser irradiation, resulting in dramatic reduction in

tumor growth (Fig. 6). The group has recently demonstrated the optimization of AuNR-mediated PPTT (in vitro) by altering the AuNR's optical properties through nanoparticle size manipulation (Mackey et al. 2014).

Another photothermally relevant gold nanoparticle that has been utilized in PPTT is the AuNc, first developed by Xia and coworkers in 2007 (Chen et al. 2007a). The AuNcs were first modified with an antibody to promote specific binding to breast cancer (SK-BR-3) cells, followed by exposure to NIR laser pulse. This resulted in the photo-thermal destruction of the cancer cells labeled with these hollow gold nanostructures. Li and coworkers, shortly thereafter, applied cancer-specific targeting AuNcs in vivo as photothermal contrast agents (Lu et al. 2009a; Melancon et al. 2008). In doing so, they were able to demonstrate the specific accumulation of AuNcs at tumor sites, as well as their external activation as photothermal contrast agents by cw NIR laser exposure, resulting in tumor destruction. While AuNCs are excellent photothermal contrast agents, they can be inherently toxic, due to the residual silver left on their interior during synthesis via galvanic replacement. The silver remaining on the inner cavity can be oxidized to silver oxide, resulting in the generation of reactive oxygen species (ROS) under physiological conditions. As Mackey et al. (2013) has shown, this toxic property can be exploited in the specific destruction of HSC-3 cancer cells, by targeting its nucleus, but one should take this into account when utilizing these particles in other biomedical applications, as adverse/nonspecific toxicity may occur. even more recently, Borghs and coworkers have synthesized branched AuNPs and modified them with nanobodies specific for breast and ovarian cancer (SKOV3) cell surface binding (Van de Broek et al. 2011). They demonstrated that upon exposure to NIR radiation, the branched AuNP-labeled cancer cells were destroyed.

Drug delivery: As discussed previously, the facile surface chemistry of AuNPs allows for their functionalization with a variety of biomolecules, making them ideal candidates as drug delivery platforms. In the past decade, scientists have made great strides in the development of AuNP drug delivery systems, not only due to their nanometer size and characteristic enhanced permeability and retention (EPR) within tumor tissue, but also their ability to bind multiple drug molecules, enhancing drug efficacy, as well as the ability to control drug release via biological stimuli (internal) or light activation (external).

The use of AuNPs in drug delivery was first demonstrated by Tamarkin, Paciotti, and coworkers, where 30 nm AuNPs were functionalized with polyethylene glycol (PEG) and tumor necrosis factor (TNF) via dative covalent attachment (Paciotti et al. 2004). These novel nanoparticles exhibited colon carcinoma (MC-38) tumor-specific accumulation and minimal systemic toxicity and, most importantly, enhanced antitumor efficacy at a lower dose than native TNF (Fig. 7). The success of this particular drug delivery platform has opened up many opportunities for the delivery of many other anticancer agents, specifically targeting tumor characteristics in a variety of cancer types. For example, targeting folate receptors overexpressed on the cancer cell surface can be done using methotrexate (MTX), which also exhibits anticancer activity. MTX can be conjugated to 13 nm AuNPs at high loading capacity (estimated ∼1,200 MTX molecules) through electrostatic interactions, as demonstrated by Chen et al. (2007b), thereby greatly enhancing MTX accumulation in Lewis lung carcinoma (LL2) tumors and subsequent antitumor activity.

Another tumor characteristic that can be targeted with AuNP drug delivery systems are hormone receptors. El-Sayed and coworkers developed two drug delivery systems: one taking advantage of the upregulated estrogen receptor in breast cancer and another targeting the upregulated androgen receptors in prostate cancer (Dreaden et al. 2009, 2012b). In targeting the estrogen receptor, the breast cancer chemotherapeutic drug, tamoxifen (TAM), was chemically modified with PEG-thiol and covalently bound to the 25 nm AuNP at an estimated 12,000 TAM molecules per particle. The nanoparticle-TAM conjugates demonstrated a 2.7-fold enhanced efficacy in human breast cancer (MCF-7) cells compared with native TAM (Dreaden et al. 2009). Much like the estrogen receptor targeting technique employed with the TAM-AuNPs, androgen receptor targeting was achieved by modifying antiandrogen chemotherapeutic agents with PEG-thiol to facilitate binding to 30 nm AuNPs. Antiandrogen therapeutic efficacy was enhanced, in chemotherapy-resistant prostate cancer (DU-145) cells, by approximately 10-fold when the antiandrogen drug molecules were modified and bound to AuNPs (Dreaden et al. 2012b).

This ability to enhance chemotherapeutic efficacy in treatment-resistant cancers is one of the primary targets for developing new drug delivery systems (Dong and Mumper 2010). One recent study, by Wang and coworkers, demonstrates enhanced doxorubicin (DOX) drug efficacy in treatment-resistant breast cancer (MCF-7/ADR) cells by modifying DOX, such that it can be attached to the 30 nm AuNP through a pH-sensitive linker (Wang et al. 2011a). This type of DOX-AuNP attachment allows for the intracellular triggered release of DOX from the AuNP once inside acidic organelles. This allowed for rapid increase in intracellular DOX concentration, thereby enhancing therapeutic effects in drug-resistant tumor cells. The concept of employing an internal, biological trigger to control drug release from a nanoparticle has been demonstrated in multiple cases. As mentioned above, the pH-triggered drug release takes advantage of the acidic nature of many intracellular organelles. Another internal trigger for drug release from AuNPs is via glutathione (GSH), an intracellular reducing agent with extremely high intracellular concentrations (1–10 mM) in comparison with that of plasma (2 μM) (Ghosh et al. 2008). This GSH gradient allows for the rapid, triggered, intracellular release of drug molecules from the AuNP, as was demonstrated by Rotello and coworkers in a proof of concept study (Hong et al. 2006). In this work, the controlled release of a fluorescent dye (representing hydrophobic drug molecules) was demonstrated after exposing the dye-loaded AuNPs to high GSH concentrations.

Not only can drug release from a AuNP be controlled by internal, biological stimuli, but also via external triggers such as light. As mentioned above, due to their unique optical properties, AuNPs can be photo-activated via radiation in the form of visible and near-infrared (NIR) light. This was first demonstrated by west and coworkers who incorporated AuNPs within a thermal-responsive polymer hydrogel containing dye molecules, representative of drug molecules (Sershen et al. 2000). Upon NIR irradiation, the plasmonic AuNPs generated heat, such that the hydrogel structure collapsed, releasing the dye molecules in a remotely triggered manner. A more detailed review of light activated drug release from AuNPs is given by Pissuwan et al. (2011).

Gene therapy: In addition to drug delivery, AuNPs offer promising platforms for nonviral gene delivery and subsequent gene regulation (i.e., gene therapy). AuNPs can potentially

help circumvent some of the barriers presented with gene delivery, including cell membrane penetration, avoiding enzymatic degradation, and efficient delivery of the intact gene to the nucleus (Wiethoff and Middaugh 2003). In 2006, Mirkin et al. demonstrated the use of 13 nm AuNPs to scavenge intracellular DNA and thereby knockdown genes within cells (termed antisense AuNPs) (Rosi et al. 2006). These DNA-AuNPs were formulated by modifying the oligodeoxynucleotides with thiol functional groups and attaching them to the AuNPs through Au–S bonds. Once introduced to cells, the DNA-AuNPs are internalized, binding complementary nucleic acids, and thereby regulating the gene of interest.

Another method by which AuNPs can be used for gene knockdown, or more specifically termed gene silencing, is by conjugation with small interfering RNA (siRNA). This technique has been demonstrated in numerous cases where an internal, biological stimulus or an external stimulus is used to trigger siRNA release from AuNPs. For example, Nagasaki and coworkers demonstrated this technique with GSH-sensitive 15 nm PEG-AuNPs bearing thiol-modified siRNA chains (Oishi et al. 2006). These siRNA-AuNPs demonstrated a GSH-triggered siRNA release from the AuNP and a subsequent increase in RNA interference (RNAi) activity to 65 % in hepatocarcinoma (HUH-7) cells, compared to that of siRNA alone (20 %). In addition to GSH-triggered RNA interference, Guo et al. (2010) recently showed that a pH trigger can enhance RNA interference, specifically when siRNA is conjugated to charge-reversal polyelectrolyte-deposited AuNPs. These novel AuNPs exhibit pH sensitivity due to their ability to change surface charge under acidic conditions (e.g., the endosome), and subsequently allowing release of siRNA to the cytoplasm of cervical cancer (Hela) cells, through endosomal membrane disruption (Fig. 8).

As previously mentioned, external stimuli with light not only can be utilized for remote-triggered release of drugs from AuNPs, but also for the controlled release of siRNA. This was shown in 2009, by Lee et al. (2009), where a thiolated sense RNA was conjugated to the AuNP and hybridized with the corresponding antisense RNA. Upon introduction of these plasmonic siRNA-AuNPs to breast cancer (BT474) cells, they were exposed to NIR radiation, causing the hybridized duplex to be heated above melting temperature, and subsequently releasing the antisense RNA to then be degraded in the cell and ultimately interfering with normal gene function.

Silver nanostructures

Antimicrobial activity: Like their Au counterparts, Ag nanostructures have been extensively used in therapeutic applications (Chaloupka et al. 2010). One of the most investigated applications is related to their antimicrobial activity. The recent increase in antibiotic-resistant bacteria, due to antibiotic overuse, has caused a need for microbicide alternatives. Since Ag compounds have readily been used in antimicrobial applications, many groups have begun investigating the antimicrobial activity of AgNPs (Rai et al. 2009; Sharma et al. 2009). In 2004, Sondi and SalopekSondi (2004) reported the antimicrobial activity of 12 nm AgNSs against *E. coli*, a gram-negative bacterium. *E.coli* was grown on agar plates and in luria–Bertani (LB) media, both containing AgNSs. TEM and SEM images revealed that agar, containing AgNSs, resulted in a concentration-dependent growth inhibition, while LB media containing AgNSs only delayed *E. coli* growth. The influence on

E. coli growth was attributed to membrane damage in the form of pits. Morones et al. (2005) further explored the antimicrobial activity of AgNPs on gram-negative bacteria and determined growth inhibition was both size and concentration-dependent. AgNPs, synthesized with a diameter of ∼16 nm, were incorporated into agar at increasing concentrations (0, 25, 50, 75, 100 μg/mL), and *E. coli* was grown on the AgNP-containing agar. At 75 μg/mL, there was no significant growth observed. High angled annular dark field (HAADF) images revealed that 5 nm AgNPs showed the greatest antimicrobial activity. Additionally, AgNPs were shown to cause growth inhibition in three ways: (1) attach to the bacteria's surface and disrupt normal function, (2) penetrate the cell membrane, and (3) release silver ions. Shape dependence on antimicrobial activity has also been studied. Song et al. prepared spherical, rod, and triangular-shaped AgNPs and assessed their antimicrobial activity against *E. coli* (Pal et al. 2007). Similar to previous works, the different shaped AgNPs were incorporated into agar plates as well as LB media. Again, it was seen that bacteria grown on agar plates showed complete growth inhibition, while LB media only resulted in a growth delay. The main contribution of this study was the revelation that antimicrobial activity was related to the AgNP shape. Triangular AgNPs showed the highest activity, followed by spheres and rods. These studies provided the foundation for AgNP antimicrobial activity, and since then, many groups have expanded upon these works (Fayaz et al. 2010; Li et al. 2010; Marambio-Jones and Hoek 2010).

Wound healing: Although AgNPs have been incorporated into many wound dressings due to their antimicrobial activity highlighted above, they also provide other beneficial properties to promote wound healing. In 2007, Tian et al. (2007) demonstrated that AgNPs topically administered to murine burn wounds accelerated healing by ∼9 days and reduced scar appearance (Fig. 9). Quickened wound healing was a result of the AgNPs' antimicrobial activity as well as a reduction in local and systemic inflammation through cytokine modulation, specifically IL-6, TGF-β1, IL-10, VEGF, and IFN-γ. The promotion of wound healing also was found to be dose-dependent. Wong and coworkers demonstrated that during wound healing, AgNPs ranging from 5 to 15 nm were able to induce different responses in keratinocyte and fibroblast skin cells (Liu et al. 2010a). Mice with induced excisional skin wounds were topically treated with AgNPs at a concentration of 0.04 mg/cm^2. Mice that received AgNP treatment resulted in wound closure ∼10 days earlier than those that received no treatment. The accelerated wound closure was attributed to the increased rate in the keratinocyte proliferation and fibroblast differentiation into myofibroblasts. Moreover, in 2011, this group reported the improvement in the tensile properties of the repaired skin (Kwan et al. 2011). This improvement was linked to the ability of AgNPs to control collagen deposition and direct collagen alignment and spatial arrangement.

Antiviral activity: AgNPs have also been shown to exhibit antiviral activity (Galdiero et al. 2011). The human immunodeficiency virus type 1 (HIV-1) is easily transmittable and extremely infective (Nyamweya et al. 2013). In 2005, Elechiguerra et al. (2005) reported the effect of AgNPs on HIV-1 and determined that infective inhibition is size-dependent. AgNPs, with diameters of 1–10 nm, were postulated to interact with the gp120 glycoprotein knobs on the viral envelope (Fig. 10a), and the degree of interaction was influenced by the

amount of capping ligand present on the AgNPs. The interaction between the HIV-1 virus and the AgNPs resulted in host cell binding inhibition of the virus (Fig. 10b). Researchers further showed that the AgNPs' inhibitory mode of action occurs via two pathways depending on whether the virus is cell-free or associated with a host cell (Lara et al. 2010b). when HIV-1 is in a cell-free form, AgNPs blocked entry into a host cell by preventing CD4-dependent viron binding and fusion, while in a cell-associated form, Ag^+ ions leached from the nanoparticle and reduce the infectivity through their interaction with various proteins, RNA and DNA. Moreover, PVP-AgNPs incorporated into a nonspermicidal gel inhibited the transmission of cell-associated and cell-free HIV-1 in human cervical culture after only 1 min of AgNP pretreatment (Lara et al. 2010a). AgNPs have also demonstrated antiviral activity against herpes simplex virus type 1 (HSV-1), the influenza virus, and the hepatitis B virus (Baram-Pinto et al. 2009; Gaikwad et al. 2013; Lu et al. 2008; Xiang et al. 2011).

Anti-angiogenesis activity: Another therapeutic use of AgNPs is as a chemotherapeutic agent. Gurunathan et al. (Gurunathan et al. 2009) reported the anti-angiogenesis activity of 50 nm AgNPs in bovine retinal epithelial cells (BREC) as well as in a matrigel mouse model. AgNPs inhibited cellular proliferation and migration in VEGF-induced angiogenesis, in BRECs, due to PI3K/Akt pathway inhibition. In another report, AgNPs were shown to have an antitumor affect against Dalton's lymphoma ascites (DLA) cell lines (Sriram et al. 2010). These AgNPs induced in vitro cell death via apoptosis in a dose-dependent manner. Apoptosis was triggered through caspase-3 enzyme activation and confirmed with nuclear fragmentation. In vivo experiments revealed that AgNPs increased the survival time by 50 %, compared to tumor controls, and decreased ascites production by 65 %. Researchers have also demonstrated the cytotoxicity of AgNPs in human breast cancer (MCF-7) cells and human lung carcinoma (A549) cells (Franco-Molina et al. 2010; Govender et al. 2012; Jeyaraj et al. 2013). AgNP cytotoxicity was attributed to DNA damage via reactive oxygen species (ROS) generation and mitochondrial depolarization. Reductions in glutathione (GSH), lactate dehydrogenase (LDH), and ATP levels were also seen. AgNPs were also used in conjunction with protoporphyrin IX (PpIX), a photosensitizer, to enhance photodynamic cancer therapy (PDT) by two orders of magnitude compared to free PpIX (Hayden et al. 2013). PDT relies on the light activation of singlet oxygen producing compounds. In this study, PDT enhancement using AgNPs, AuNRs, and AuNPs was assessed. AgNPs showed the greatest cytotoxicity when PpIX was covalently attached to the surface. PDT enhancement was attributed to the spectral overlap between the LSPR of the AgNPs and PpIX, which increased the quantum yield of singlet oxygen produced by PpIX.

Clinical applications

Biodiagnostics

Localized surface plasmon resonance assays: Lateral-flow assays comprise one of the earliest modern clinical applications of noble metal nanoparticles in biomedicine (Fig. 11a) (Mark et al. 2010). Here, a solution is wicked onto a test strip, and the presence of an analyte is indicated by the localized appearance of a colored band. In the First Response™ pregnancy exam (Carter-Wallace), the biomarker human chorionic gonadotropin (hCG) is detected in urine. In this application, urine is sorbed onto a test strip and directed toward a reservoir containing gold nanoparticle-anti-hCG conjugates. hCG binds the brightly colored

nanoparticles and wicks up the test strip to a detection site containing immobilized anti-hCG. This antibody-sandwiched hCG thus appears as a distinct red band. Gold nanoparticles are particularly useful in these types of assays; unlike molecular fluorophores, which are prone to photobleaching, AuNPs are indefinitely photostable and absorb visible light approximately one million times more strongly than an equal number of rhodamine dye molecules.

Additional applications of AuNP-based lateral flow assays include the detection and monitoring of food-borne pathogens. verotoxin, or Shiga-like toxin, produced by enterohaemorrhagic escherichia coli (EHEC), is a common contaminant in cantaloupe, as well as alfalfa and radish sprouts, and can cause hemolytic anemia, thrombopenia, and kidney failure following exposure (Bae et al. 2006). The Duopath™ lateral flow assay (Merck KGaA) can detect verotoxin with sensitivities equal to that of culture analyses, ELISA, or PCR, and can be performed in the field without specialized equipment or personnel in just 20 min (Park et al. 2003). Allergic hypersensitivity (atopic syndrome) represents another AuNP-enabled rapid test application. The ImmunoCAP™ Rapid test (Phadia, Inc) can detect IgE associated with 10 distinct allergens from blood in as little as 20 min, aiding in the identification and diagnosis of potentially life-threatening allergies in children (Diaz-Vazquez et al. 2009; Johansson 2004). Other emerging AuNP-enabled applications include the detection of nucleic acids, vaccine-associated antibodies against biological warfare agents, sexually transmitted diseases (herpes simplex virus type 2), microbial drinking water contaminants, prescription drug metabolites (benzodiazepins), and other food-borne pathogens (Biagini et al. 2006; Mao et al. 2009; Laderman et al. 2008; Li et al. 2009; Lindhardt et al. 2009; Rong-Hwa et al. 2010; Tippkotter et al. 2009).

Rayleigh and Raman scattering: The Verigene™ diagnostic platform (Nanosphere Inc.) uses oligonucleotide-functionalized gold nanoparticles to detect genomic DNA, RNA, or proteins from complex media based on Ag amplification and optical scattering from particles bound to oligonucleotide arrays (Fig. 11b) (Lefferts et al. 2009). The method has been approved to determine patient sensitivity to the blood thinner, warfarin, based on genotyping of the *2 and *3 alleles of the *CYP2C19* gene locus and point mutation analysis (C1173T) at the *VKORC1* gene locus (Richmond 2008). The methodology is additionally approved to detect respiratory infections (RSV A/B, influenza A/B, 2009 H1N1), gastrointestinal infections (Clostridium difficile bacteria), and sepsis (genus, species, and genetic resistance determinants for gram-positive/negative bacteria), with potential future applications in the detection of oncogenes, cancer biomarkers, biological warfare agents, and Alzheimer's. while less well-developed than optical scattering bioassays, SERS-based enzyme-linked immunosorbent assays (ELISAs) (Sword Diagnostics), nanostructured Au and Ag substrates for reproducible SERS measurements (Klarite™, Renishaw; SERStrate™, Silmeco) (Fig. 11c), and platforms for SERS image-guided surgery (Spectropen™, Spectropath Inc) (Fig. 11d) are rapidly growing areas for research commercialization (Mohs et al. 2010; Schmidt et al. 2012).

Other properties: Due to their high electron density and capacity for distance-dependent resonant energy transfer, Au and Ag nanostructures exhibit additional properties useful in

biodiagnostics. These structures can be used to detect intracellular mRNA through quenching of fluorophore-bound oligonucleotides displaced following binding of target RNA strands (SmartFlare™, Millipore Inc) (Fig. 11e) (Seferos et al. 2007). Likewise, antibody- and streptavidin-based imaging probes for electron microscopy (Nanogold™, Nanoprobes, Inc) (Fig. 11f) provide opportunities for basic clinical research, while AuNP-based contrast agents for X-ray computed tomography (Aurovist™, Nanoprobes Inc) exhibit promising preclinical findings (Graf et al. 2000).

Therapy

Photothermal therapy: The efficient conversion of light into heat using Au and Ag nanostructures of discreet size/shape provides a range of opportunities in laser-assisted tissue ablation therapies (Dreaden et al. 2012a; Dreaden and El-Sayed 2012). Aurolase™ (Nanospectra Biosciences) exploits the near-infrared absorption of silica–gold core–shell nanoparticles to achieve tumor-targeted laser photothermal ablation of a variety of solid tumors (Fig. 12c). Human pilot studies for the treatment of head and neck tumors were set to be completed by Dec 2013 (NCT00848042), with a pilot study for the treatment of lung carcinoma tumors by optical fiber bronchoscopy currently in progress (NCT01679470). Trials investigating the ablation of atherosclerotic plaques have also been conducted (NCT01436123, NCT01270139). Interestingly, tumor-specific laser exposure has also been used to augment the tissue-specific accumulation of gold nanorods in tumor-bearing mice; this method has yet to be explored in a clinical setting (Shiotani et al. 2010).

Drug delivery: One of the earliest modern therapeutic applications of noble metal nanostructures centered around the discovery that AuNPs could significantly improve tissue disposition, tumor accumulation, and the therapeutic index of tumor necrosis factor alpha (TNFα) therapy (Fig. 12a) (Paciotti et al. 2001, 2006). Although systemic delivery of the antitumor cytokine was previously limited due to acute immune response, Aurimmune™, a TNFα gold nanoparticle conjugate, demonstrated safety and tolerability in recent phase I clinical trials (NCT00356980, NCT00436410) (Libutti et al. 2009, 2010). The drug's development company, CytImmune, Inc, recently announced a partnership with pharma giant AstraZeneca to further develop the gold nanoparticle delivery platform for combination cytotoxic chemotherapy.

In addition to systemic delivery, the high stability of Au nanostructures can also be utilized in transdermal delivery applications where the particle acts as a scaffold for antigen delivery to highly immuno-responsive subdermal tissues. Transdermal gene gun technology was initially developed by PowderMed and later acquired by Pfizer in 2006. The company's disposable delivery device, ND10, which uses high-pressure He to deliver DNA vaccine-AuNP conjugates, demonstrated significant protection against monkey-pox virus, a potential biological warfare agent, in nonhuman primates (Fig. 12b) (Golden et al. 2012). In a phase I clinical trial investigating immunization against hemorrhagic fever with renal syndrome (HFRS)—caused by hantaviruses—immunization against Hantaan (HTNV) and Puumala (PUUV) viruses (8 μg DNA/4 mg gold/patient) was safe and exhibited strong neutralizing antibody response in humans (Boudreau et al. 2012). A human papilloma virus (HPV) DNA vaccine phase I clinical trial is also currently in preparation for the treatment of HPV-16-

positive cervical carcinoma using a DNA vaccine encoding cal-reticulin (CRT) fused to HPv-16 E7 (E7detox) (Huang et al. 2010).

Conclusion

As highlighted in this review, there has been significant interest and research conducted on Au and Ag nanostructures for biodiagnostic, imaging, therapeutic, and drug delivery applications. Their biologically relevant size, ability to easily functionalize with biomolecules and chemo-therapeutic agents, as well as their enhanced optical properties aids in their ability to improve therapeutic delivery and noninvasive disease diagnostics. In order for their successful use in biomedical applications, Au and Ag nanostructures' long-term cytotoxicity and genotoxicity should be evaluated. Nevertheless, the accomplishments in this review demonstrate the significant impact that nanotechnology has had on the biomedical field.

Acknowledgments

MAE and coworkers would like to acknowledge the support from the U.S. National Institutes of Health (1U01CA151802-01). LAA thanks the support from Georgia Institute of Technology/Department of education's Graduate Assistance in Areas of National Need (GAANN) Molecular Biophysics and Biotechnology Fellowship. ECD acknowledges postdoctoral fellowship support from the NIH (Ruth L. Kirschstein NRSA 1F32EB017614-01).

References

Ali MRK, Snyder B, El-Sayed MA. Synthesis and optical properties of small Au nanorods using a seedless growth technique. Langmuir. 2012; 28(25):9807–9815.10.1021/la301387p [PubMed: 22620850]

Alivisatos AP, Johnsson KP, Peng XG, et al. Organization of ‘nanocrystal molecules’ using DNA. Nature. 1996; 382(6592):609–611.10.1038/382609a0 [PubMed: 8757130]

Amoozgar Z, Yeo Y. Recent advances in stealth coating of nanoparticle drug delivery systems. Wiley Interdiscip Rev Nanomed Nanobiotechnol. 2012; 4(2):219–233.10.1002/wnan.1157 [PubMed: 22231928]

Arvizo RR, Bhattacharyya S, Kudgus RA, Giri K, Bhattacharya R, Mukherjee P. Intrinsic therapeutic applications of noble metal nanoparticles: past, present and future. Chem Soc Rev. 2012; 41(7): 2943–2970.10.1039/c2cs15355f [PubMed: 22388295]

Aslan K, Lakowicz JR, Geddes CD. Nanogold-plasmon-resonance-based glucose sensing. Anal Biochem. 2004; 330(1):145–155.10.1016/j.ab.2004.03.032 [PubMed: 15183773]

Aslan K, Gryczynski I, Malicka J, Matveeva E, Lakowicz JR, Geddes CD. Metal-enhanced fluorescence: an emerging tool in biotechnology. Curr Opin Biotechnol. 2005; 16(1):55–62. [PubMed: 15722016]

Aslan K, Huang J, Wilson GM, Geddes CD. Metal-enhanced fluorescence-based RNA sensing. J Am Chem Soc. 2006; 128(13):4206–4207.10.1021/ja0601179 [PubMed: 16568977]

Atkinson R, Zhang M, Diagaradjane P, et al. Thermal enhancement with optically activated gold nanoshells sensitizes breast cancer stem cells to radiation therapy. Sci Trans Med. 2010; 2(55) 10.1126/scitranslmed.3001447.

Austin LA, Kang B, Yen CW, El-Sayed MA. Nuclear targeted silver nanospheres perturb the cancer cell cycle differently than those of nanogold. Bioconjugate Chem. 2011a; 22(11):2324–2331.10.1021/bc200386m

Austin LA, Kang B, Yen CW, El-Sayed MA. Plasmonic imaging of human oral cancer cell communities during programmed cell death by nuclear-targeting silver nanoparticles. J Am Chem Soc. 2011b; 133(44):17594–17597.10.1021/ja207807t [PubMed: 21981727]

Austin LA, Kang B, El-Sayed MA. A new nanotechnology technique for determining drug efficacy using targeted plasmonically enhanced single cell imaging spectroscopy. J Am Chem Soc. 2013; 135(12):4688–4691.10.1021/ja4011145 [PubMed: 23469948]

Bae WK, Lee YK, Cho MS, et al. A case of hemolytic uremic syndrome caused by *Escherichia coli* O104:H4. Yonsei Med J. 2006; 47(3):437–439. [PubMed: 16807997]

Baram-Pinto D, Shukla S, Perkas N, Gedanken A, Sarid R. Inhibition of herpes simplex virus type 1 infection by silver nanoparticles capped with mercaptoethane sulfonate. Bioconjugate Chem. 2009; 20(8):1497–1502.10.1021/bc900215b

Baron R, Zayats M, Willner L. Dopamine-, l-DOPA-, adrenaline-, and noradrenaline-induced growth of au nanoparticles: assays for the detection of neurotransmitters and of tyrosinase activity. Anal Chem. 2005; 77(6):1566–1571.10.1021/ac048691v [PubMed: 15762558]

Bert HPW, Olaf A, Annette D, Geetha S, Thoralf K, Roland F, Hanno R. Crit Rev Oncol/Hematol. 2002; 43:33–56.

Bharill S, Chen C, Stevens B, et al. Enhancement of single-molecule fluorescence signals by colloidal silver nanoparticles in studies of protein translation. ACS Nano. 2010; 5(1):399–407.10.1021/nn101839t [PubMed: 21158483]

Bhowmick S, Saini S, Shenoy VB, Bagchi B. Resonance energy transfer from a fluorescent dye to a metal nanoparticle. J Chem Phys. 2006; 125(18):181102. [PubMed: 17115730]

Biagini RE, Sammons DL, Smith JP, et al. Rapid, sensitive, and specific lateral-flow immunochromatographic device to measure anti-anthrax protective antigen immunoglobulin G in serum and whole blood. Clin Vaccine Immunol. 2006; 13(5):541–546.10.1128/cvi.13.5.541-546.2006 [PubMed: 16682473]

Boisselier E, Astruc D. Gold nanoparticles in nanomedicine: preparations, imaging, diagnostics, therapies and toxicity. Chem Soc Rev. 2009; 38(6):1759–1782.10.1039/b806051g [PubMed: 19587967]

Boudreau E, Josleyn M, Ullman D, et al. A Phase 1 clinical trial of Hantaan virus and Puumala virus M-segment DNA vaccines for hemorrhagic fever with renal syndrome. Vaccine. 2012; 30(11): 1951–1958.10.1016/j.vaccine.2012.01.024 [PubMed: 22248821]

Brust M, Walker M, Bethell D, Schiffrin DJ, Whyman R. Synthesis of thiol-derivatised gold nanoparticles in a two-phase liquid–liquid system. J Chem Soc Chem Commun. 1994; 7:801–802. 10.1039/c39940000801.

Caro C, Castillo PM, Klippstein R, Pozo D, Zaderenko AP. Silver nanoparticles: sensing and imaging applications. Silver nanoparticles: AP. 2010

Chaloupka K, Malam Y, Seifalian AM. Nanosilver as a new generation of nanoproduct in biomedical applications. Trends Biotechnol. 2010; 28(11):580–588.10.1016/j.tibtech.2010.07.006 [PubMed: 20724010]

Chen J, Saeki F, Wiley BJ, et al. Gold nanocages: bioconjugation and their potential use as optical imaging contrast agents. Nano Lett. 2005; 5(3):473–477.10.1021/nl047950t [PubMed: 15755097]

Chen J, Mclellan JM, Siekkinen A, Xiong Y, Li ZY, Xia Y. Facile synthesis of gold–silver nanocages with controllable pores on the surface. J Am Chem Soc. 2006; 128(46):14776–14777.10.1021/ja066023g [PubMed: 17105266]

Chen J, Wang D, Xi J, et al. Immuno gold nanocages with tailored optical properties for targeted photothermal destruction of cancer cells. Nano Lett. 2007a; 7(5):1318–1322.10.1021/nl070345g [PubMed: 17430005]

Chen YH, Tsai CY, Huang PY, et al. Methotrexate conjugated to gold nanoparticles inhibits tumor growth in a syngeneic lung tumor model. Mol Pharm. 2007b; 4(5):713–722.10.1021/Mp060132k [PubMed: 17708653]

Chen G, Song F, Xiong X, Peng X. Fluorescent nanosensors based on fluorescence resonance energy transfer (FRET). Ind Eng Chem Res. 2013; 52(33):11228–11245.10.1021/ie303485n

Choi Y, Choi JH, Liu L, Oh BK, Park S. Optical sensitivity comparison of multiblock gold-silver nanorods toward biomolecule detection: quadrupole surface plasmonic detection of dopamine. Chem Mater. 2013; 25(6):919–926.10.1021/cm304030r

Dai Q, Liu X, Coutts J, Austin L, Huo Q. A one-step highly sensitive method for DNA detection using dynamic light scattering. J Am Chem Soc. 2008; 130(26):8138–8139.10.1021/ja801947e [PubMed: 18540598]

Diaz-Vazquez C, Torregrosa-Bertet MJ, Carvajal-Urueña I, et al. Accuracy of ImmunoCAP® Rapid in the diagnosis of allergic sensitization in children between 1 and 14 years with recurrent wheezing: the IReNE study. Pediatr Allergy Immunol. 2009; 20(6):601–609.10.1111/j.1399-3038.2008.00827.x [PubMed: 19220775]

Dickerson EB, Dreaden EC, Huang X, et al. Gold nanorod assisted near-infrared plasmonic photothermal therapy (PPTT) of squamous cell carcinoma in mice. Cancer Lett. 2008; 269(1):57–66.10.1016/j.canlet.2008.04.026 [PubMed: 18541363]

Dong XW, Mumper RJ. Nanomedicinal strategies to treat multidrug-resistant tumors: current progress. Nanomedicine. 2010; 5(4):597–615.10.2217/Nnm.10.35 [PubMed: 20528455]

Dreaden EC, El-Sayed MA. Detecting and destroying cancer cells in more than one way with noble metals and different confinement properties on the nanoscale. Acc Chem Res. 2012; 45(11):1854–1865. [PubMed: 22546051]

Dreaden EC, Mwakwari SC, Sodji QH, Oyelere AK, El-Sayed MA. Tamoxifen-poly(ethylene glycol)-thiol gold nanoparticle conjugates: enhanced potency and selective delivery for breast cancer treatment. Bioconjugate Chem. 2009; 20(12):2247–2253.10.1021/Bc9002212

Dreaden EC, Mackey MA, Huang X, Kang B, El-Sayed MA. Beating cancer in multiple ways using nanogold. Chem Soc Rev. 2011; 40(7):3391–3404. [PubMed: 21629885]

Dreaden EC, Alkilany AM, Huang X, Murphy CJ, El-Sayed MA. The golden age: gold nanoparticles for biomedicine. Chem Soc Rev. 2012a; 41(7):2740–2779. [PubMed: 22109657]

Dreaden EC, Gryder BE, Austin LA, et al. Antiandrogen gold nanoparticles dual-target and overcome treatment resistance in hormone-insensitive prostate cancer cells. Bioconjugate Chem. 2012b; 23(8):1507–1512.10.1021/Bc300158k

Du BA, Li ZP, Cheng YQ. Homogeneous immunoassay based on aggregation of antibody-functionalized gold nanoparticles coupled with light scattering detection. Talanta. 2008; 75(4):959–964.10.1016/j.talanta.2007.12.048 [PubMed: 18585169]

Dubois LH, Nuzzo RG. Synthesis, structure, and properties of model organic surfaces. Annu Rev Phys Chem. 1992; 43(1):437–463.10.1146/annurev.pc.43.100192.002253

Dulkeith E, Ringler M, Klar TA, Feldmann J, Muoz Javier A, Parak WJ. Gold nanoparticles quench fluorescence by phase induced radiative rate suppression. Nano Lett. 2005; 5(4):585–589.10.1021/nl0480969 [PubMed: 15826091]

Elechiguerra JL, Burt JL, Morones JR, et al. Interaction of silver nanoparticles with HIV-1. J Nanobiotechnol. 2005; 3(6):1–10.

Elghanian R, Storhoff JJ, Mucic RC, Letsinger RL, Mirkin CA. Selective colorimetric detection of polynucleotides based on the distance-dependent optical properties of gold nanoparticles. Science. 1997; 277(5329):1078–1081.10.1126/science.277.5329.1078 [PubMed: 9262471]

El-Sayed MA. Some interesting properties of metals confined in time and nanometer space of different shapes. Acc Chem Res. 2001; 34(4):257–264. [PubMed: 11308299]

El-Sayed IH, Huang XH, El-Sayed MA. Surface plasmon resonance scattering and absorption of anti-EGFR antibody conjugated gold nanoparticles in cancer diagnostics: applications in oral cancer. Nano Lett. 2005; 5(5):829–834.10.1021/nl050074e [PubMed: 15884879]

Englebienne P. Use of colloidal gold surface plasmon resonance peak shift to infer affinity constants from the interactions between protein antigens and antibodies specific for single or multiple epitopes. Analyst. 1998; 123(7):1599–1603.10.1039/a804010i [PubMed: 9830172]

Fang Y. Optical absorption of nanoscale colloidal silver: aggregate band and adsorbate-silver surface band. J Chem Phys. 1998; 108(10):4315–4318.10.1063/1.475831

Faraday M. The Bakerian lecture: experimental relations of gold (and Other Metals) to light. Philos Trans R Soc London. 1857; 147:145–181.10.1098/rstl.1857.0011

Fayaz AM, Balaji K, Girilal M, Yadav R, Kalaichelvan PT, Venketesan R. Biogenic synthesis of silver nanoparticles and their synergistic effect with antibiotics: a study against gram-positive and gram-negative bacteria. Nanomed Nanotechnol Biol Med. 2010; 6(1):103–109.10.1016/j.nano.2009.04.006

Fischler M, Sologubenko A, Mayer J, et al. Chain-like assembly of gold nanoparticles on artificial DNA templates via ‘click chemistry’. Chem Commun. 2008; 2:169–171. 10.1039/b715602b.

Franco-Molina MA, Mendoza-Gamboa E, Sierra-Rivera CA, et al. Antitumor activity of colloidal silver on McF-7 human breast cancer cells. J Exp Clin Cancer Res. 2010; 29(1):148. [PubMed: 21080962]

Frens G. Controlled nucleation for the regulation of the particle size in monodisperse gold suspensions. Nature. 1973; 241:20–22.10.1038/physci241020a0

Gaikwad S, Ingle A, Gade A, et al. Antiviral activity of myco-synthesized silver nanoparticles against herpes simplex virus and human parainfluenza virus type 3. Int J Nanomed. 2013; 8:4303–4314.10.2147/ijn.s50070

Galdiero S, Falanga A, Vitiello M, Cantisani M, Marra V, Galdiero M. Silver nanoparticles as potential antiviral agents. Molecules. 2011; 16(10):8894–8918. [PubMed: 22024958]

Ghosh P, Han G, De M, Kim CK, Rotello VM. Gold nano-particles in delivery applications. Adv Drug Delivery Rev. 2008; 60(11):1307–1315.10.1016/j.addr.2008.03.016

Glynou K, Ioannou PC, Christopoulos TK, Syriopoulou V. Oligonucleotide-functionalized gold nanoparticles as probes in a dry-reagent strip biosensor for DNA analysis by hybridization. Anal Chem. 2003; 75(16):4155–4160.10.1021/ac034256+ [PubMed: 14632129]

Golden J, Josleyn M, Mucker E, et al. Side-by-side comparison of gene-based smallpox vaccine with MvA in nonhuman primates. PloS ONE. 2012; 7(7)10.1371/journal.pone.0042353

Govender R, Phulukdaree A, Gengan RM, Anand K, Chuturgoon AA. Silver nanoparticles of Albizia Adianthifolia: the induction of apoptosis in a human lung carcinoma cell line. J Nanobiotechnol. 2012; 11(5):1–9.10.1186/1477-3155-11-5

Graf AH, Cheung AL, Hauser-Kronberger C, et al. Clinical relevance of HPv 16/18 testing methods in cervical squamous cell carcinoma. Appl Immunohistochem Mol Morphol. 2000; 8(4):300–309. [PubMed: 11127922]

Griffin J, Singh AK, Senapati D, et al. Size- and distance-dependent nanoparticle surface-energy transfer (NSET) Method for selective sensing of hepatitis C virus RNA. Chem Eur J. 2009; 15(2):342–351.10.1002/chem.200801812 [PubMed: 19035615]

Grubisha DS, Lipert RJ, Park HY, Driskell J, Porter MD. Femtomolar detection of prostate-specific antigen: an immunoassay based on surface-enhanced Raman scattering and immunogold labels. Anal Chem. 2003; 75(21):5936–5943.10.1021/ac034356f [PubMed: 14588035]

Grzelczak M, Perez-Juste J, Mulvaney P, Liz-Marzan LM. Shape control in gold nanoparticle synthesis. Chem Soc Rev. 2008; 37(9):1783–1791.10.1039/b711490g [PubMed: 18762828]

Guo ST, Huang YY, Jiang QA, et al. Enhanced gene delivery and siRNA silencing by gold nanoparticles coated with charge-reversal polyelectrolyte. ACS Nano. 2010; 4(9):5505–5511.10.1021/Nn101638u [PubMed: 20707386]

Gurunathan S, Lee KJ, Kalishwaralal K, Sheikpranbabu S, Vaidyanathan R, Eom SH. Antiangiogenic properties of silver nanoparticles. Biomaterials. 2009; 30(31):6341–6350. [PubMed: 19698986]

Haes AJ, Hall WP, Chang L, Klein WL, Van Duyne RP. A localized surface plasmon resonance biosensor: first steps toward an assay for Alzheimer's disease. Nano Lett. 2004a; 4(6):1029–1034.10.1021/nl049670j

Haes AJ, Zou S, Schatz GC, Van Duyne RP. Nanoscale optical biosensor: short range distance dependence of the localized surface plasmon resonance of noble metal nanoparticles. J Phys Chem B. 2004b; 108(22):6961–6968.10.1021/jp036261n

Hayden SC, Austin LA, Near RD, Ozturk R, El-Sayed MA. Plasmonic enhancement of photodynamic cancer therapy. J Photochem Photobiol, A. 2013; 269:34–41.

Hirsch LR, Stafford RJ, Bankson JA, et al. Nanoshell-mediated near-infrared thermal therapy of tumors under magnetic resonance guidance. Proc Natl Acad Sci USA. 2003; 100(23):13549–13554.10.1073/pnas.2232479100 [PubMed: 14597719]

Hong R, Han G, Fernandez JM, Kim BJ, Forbes NS, Rotello VM. Glutathione-mediated delivery and release using monolayer protected nanoparticle carriers. J Am Chem Soc. 2006; 128(4):1078–1079.10.1021/Ja056726 [PubMed: 16433515]

Höppener C, Novotny L. Exploiting the light–metal interaction for biomolecular sensing and imaging. Quart Rev Biophys. 2012; 45(02):209–255.10.1017/S0033583512000042

Hsin-Neng W, Tuan VD. Multiplex detection of breast cancer biomarkers using plasmonic molecular sentinel nanoprobes. Nanotechnology. 2009; 20(6):065101. [PubMed: 19417369]

Huang X, El-Sayed IH, Qian W, El-Sayed MA. Cancer cell imaging and photothermal therapy in the near-infrared region by using gold nanorods. J Am Chem Soc. 2006a; 128(6):2115–2120.10.1021/ja057254a [PubMed: 16464114]

Huang XH, Jain PK, El-Sayed IH, El-Sayed MA. Determination of the minimum temperature required for selective photothermal destruction of cancer cells with the use of immunotargeted gold nanoparticles. Photochem Photobiol. 2006b; 82(2):412–417.10.1562/2005-12-14-ra-754 [PubMed: 16613493]

Huang X, El-Sayed IH, Qian W, El-Sayed MA. Cancer cells assemble and align gold nanorods conjugated to antibodies to produce highly enhanced, sharp, and polarized surface Raman spectra: a potential cancer diagnostic marker. Nano Lett. 2007; 7(6):1591–1597.10.1021/nl070472c [PubMed: 17474783]

Huang XH, Jain PK, El-Sayed IH, El-Sayed MA. Plasmonic photothermal therapy (PPTT) using gold nanoparticles. Lasers Med Sci. 2008; 23(3):217–228.10.1007/s10103-007-0470-x [PubMed: 17674122]

Huang X, Neretina S, El-Sayed MA. Gold nanorods: from synthesis and properties to biological and biomedical applications. Adv Mater. 2009; 21(48):4880–4910.10.1002/adma.200802789

Huang CF, Monie A, Weng WH, Wu T. DNA vaccines for cervical cancer. Am J Trans Res. 2010; 2(1):75–87.

Iyer AK, Khaled G, Fang J, Maeda H. Exploiting the enhanced permeability and retention effect for tumor targeting. Drug Discov Today. 2006; 11(17–18):812–818.10.1016/j.drudis.2006.07.005 [PubMed: 16935749]

Jain PK, Eustis S, El-Sayed MA. Plasmon coupling in nanorod assemblies: optical absorption, discrete dipole approximation simulation, and exciton-coupling model. J Phys Chem B. 2006; 110(37): 18243–18253.10.1021/jp063879z [PubMed: 16970442]

Jain PK, Huang X, El-Sayed IH, El-Sayad MA. Review of some interesting surface plasmon resonance-enhanced properties of noble metal nanoparticles and their applications to biosystems. Plasmonics. 2007; 2(3):107–118.10.1007/s11468-007-9031-1

Jain PK, Huang XH, El-Sayed IH, El-Sayed MA. Noble metals on the nanoscale: optical and photothermal properties and some applications in imaging, sensing, biology, and medicine. Acc Chem Res. 2008; 41(12):1578–1586.10.1021/ar7002804 [PubMed: 18447366]

Jana NR, Gearheart L, Murphy CJ. Seed-mediated growth approach for shape-controlled synthesis of spheroidal and rod-like gold nanoparticles using a surfactant template. Adv Mater. 2001a; 13(18): 1389–1393.10.1002/1521-4095(200109)13:18<1389:aid-adma1389>3.0.co;2-f

Jana NR, Gearheart L, Murphy CJ. Wet chemical synthesis of high aspect ratio cylindrical gold nanorods. J Phys Chem B. 2001b; 105(19):4065–4067.10.1021/jp0107964

Jana NR, Gearheart L, Murphy CJ. Wet chemical synthesis of silver nanorods and nanowires of controllable aspect ratio. Chem Commun. 2001c; 7:617–618. 10.1039/b100521i.

Jans H, liu X, Austin L, Maes G, Huo Q. Dynamic light scattering as a powerful tool for gold nanoparticle bioconjugation and biomolecular binding studies. Anal Chem. 2009; 81(22):9425–9432.10.1021/ac901822w [PubMed: 19803497]

Jennings TL, Singh MP, Strouse GF. Fluorescent lifetime quenching near d = 1.5 nm gold nanoparticles:Ää probing NSET validity. J Am Chem Soc. 2006; 128(16):5462–5467.10.1021/ja0583665 [PubMed: 16620118]

Jeong E, Jung G, Hong C, Lee H. Gold nanoparticle (AuNP)-based drug delivery and molecular imaging for biomedical applications. Arch Pharmacal Res. 2014; 37(1):53–59.10.1007/s12272-013-0273-5

Jeyaraj M, Sathishkumar G, Sivanandhan G, et al. Biogenic silver nanoparticles for cancer treatment: an experimental report. Colloids Surf B. 2013; 106:86–92.

Johansson S. ImmunoCAP® specific IgE test: an objective tool for research and routine allergy diagnosis. Expert Rev Molec Diagn. 2004; 4(3):273–279. [PubMed: 15137895]

Jokerst JV, Cole AJ, Van de Sompel D, Gambhir SS. Gold nanorods for ovarian cancer detection with photoacoustic imaging and resection guidance via Raman imaging in living mice. ACS Nano. 2012; 6(11):10366–10377.10.1021/nn304347g [PubMed: 23101432]

Ju, H.; Zhang, X.; Wang, J. Biological and medical physics, biomedical engineering. Springer; New York: 2011. Biofunctionalization of nanomaterials nanobiosensing; p. 1-38.

Jue, T., editor. Biomedical applications of biophysics. Springer; New York: 2010.

Kang B, Mackey MA, El-Sayed MA. Nuclear targeting of gold nanoparticles in cancer cells induces DNA damage, causing cytokinesis arrest and apoptosis. J Am Chem Soc. 2010a; 132(5):1517–1519.10.1021/ja9102698 [PubMed: 20085324]

Kang T, Yoo SM, Yoon I, Lee SY, Kim B. Patterned multiplex pathogen DNA detection by au particle-on-wire SERS sensor. Nano Lett. 2010b; 10(4):1189–1193.10.1021/nl1000086 [PubMed: 20222740]

Kang B, Austin LA, El-Sayed MA. Real-time molecular imaging throughout the entire cell cycle by targeted plasmonic-enhanced rayleigh/raman spectroscopy. Nano Lett. 2012; 12(10):5369–5375.10.1021/nl3027586 [PubMed: 22978570]

Keren S, Zavaleta C, Cheng Z, de la Zerda A, Gheysens O, Gambhir SS. Noninvasive molecular imaging of small living subjects using Raman spectroscopy. Proc Natl Acad Sci. 2008; 105(15):5844–5849.10.1073/pnas.0710575105 [PubMed: 18378895]

Kim CK, Ghosh P, Pagliuca C, Zhu ZJ, Menichetti S, Rotello VM. Entrapment of hydrophobic drugs in nanoparticle monolayers with efficient release into cancer cells. J Am Chem Soc. 2009; 131(4):1360–1361.10.1021/ja808137c [PubMed: 19133720]

Kneipp K, Kneipp H, Kartha VB, et al. Detection and identification of a single DNA base molecule using surface-enhanced Raman scattering (SERS). Phys Rev E Stat Nonlinear Soft Matter Phys. 1998; 57(6):R6281–R6284.10.1103/PhysReve.57.R6281

Kneipp K, Haka AS, Kneipp H, et al. Surface-enhanced Raman spectroscopy in single living cells using gold nanoparticles. Appl Spectrosc. 2002; 56(2):150–154.10.1366/0003702021954557

Kneipp J, Kneipp H, Mclaughlin M, Brown D, Kneipp K. In vivo molecular probing of cellular compartments with gold nanoparticles and nanoaggregates. Nano Lett. 2006; 6(10):2225–2231.10.1021/nl061517x [PubMed: 17034088]

Kneipp J, Kneipp H, Wittig B, Kneipp K. Novel optical nanosensors for probing and imaging live cells. Nanomed Nanotechnol Biol Med. 2010; 6(2):214–226.10.1016/j.nano.2009.07.009

Kumar A, Zhang X, Liang XJ. Gold nanoparticles: emerging paradigm for targeted drug delivery system. Biotechnol Adv. 2013; 31(5):593–606.10.1016/j.biotechadv.2012.10.002 [PubMed: 23111203]

Kwan KH, Liu X, To MK, Yeung KW, Ho Cm, Wong KK. Modulation of collagen alignment by silver nanoparticles results in better mechanical properties in wound healing. Nanomed Nanotechnol Biol Med. 2011; 7(4):497–504.

Laderman EI, Whitworth E, Dumaual E, et al. Rapid, sensitive, and specific lateral-flow immunochromatographic point-of-care device for detection of herpes simplex virus type 2-specific immunoglobulin G antibodies in serum and whole blood. Clin Vaccine Immunol. 2008; 15(1):159–163.10.1128/cvi.00218-07 [PubMed: 18003814]

Lakowicz J. Plasmonics in biology and plasmon-controlled fluorescence. Plasmonics. 2006; 1(1):5–33.10.1007/s11468-005-9002-3 [PubMed: 19890454]

Lara H, Ixtepan-Turrent L, Garza-Trevino E, Rodriguez-Padilla C. PVP-coated silver nanoparticles block the transmission of cell-free and cell-associated HIV-1 in human cervical culture. J Nanobiotechnol. 2010a; 8(1):15.

Lara HH, Ayala-Nuñez NV, Ixtepan-Turrent L, Rodriguez-Padilla C. Mode of antiviral action of silver nanoparticles against HIV-1. J Nanobiotechnol. 2010b; 8(1):1–8.

Lee KS, El-Sayed MA. Gold and silver nanoparticles in sensing and imaging: sensitivity of plasmon response to size, shape, and metal composition. J Phys Chem B. 2006; 110(39):19220–19225.10.1021/jp062536y [PubMed: 17004772]

Lee JS, Han MS, Mirkin CA. Colorimetric detection of mercuric ion (Hg2 +) in aqueous media using DNA-functionalized gold nanoparticles. Angew Chem Int Ed. 2007; 46(22):4093–4096.10.1002/anie.200700269

Lee SE, Liu GL, Kim F, Lee LP. Remote optical switch for localized and selective control of gene interference. Nano Lett. 2009; 9(2):562–570.10.1021/Nl802689k [PubMed: 19128006]

Lee S, Chon H, Lee J, et al. Rapid and sensitive phenotypic marker detection on breast cancer cells using surface-enhanced Raman scattering (SERS) imaging. Biosens Bioelectron. 2014; 51:238–243.10.1016/j.bios.2013.07.063 [PubMed: 23973735]

Lefferts J, Jannetto P, Tsongalis G. Evaluation of the nanosphere verigene system and the verigene F5/F2/MTHFR nucleic acid tests. Exp Mol Pathol. 2009; 87(2):105–108.10.1016/j.yexmp.2009.06.002 [PubMed: 19573527]

Li Q, Liu L, Chen W, Peng C, Wang L, Xu C. Gold nanoparticle-based immunochromatographic assay for the detection of 7-aminoclonazepam in urine. Int J Environ Anal Chem. 2009; 89(4):261–268.10.1080/03067310802538493

Li WR, Xie XB, Shi QS, Zeng HY, Ou-Yang YS, Chen YB. Antibacterial activity and mechanism of silver nanoparticles on escherichia coli. Appl Microbiol Biotechnol. 2010; 85(4):1115–1122.10.1007/s00253-009-2159-5 [PubMed: 19669753]

Li Y, Jing C, Zhang L, Long YT. Resonance scattering particles as biological nanosensors in vitro and in vivo. Chem Soc Rev. 2012; 41(2):632–642.10.1039/c1cs15143f [PubMed: 21853183]

Libutti SK, Paciotti GF, Myer L, et al. Results of a completed phase I clinical trial of cYT-6091: a pegylated colloidal gold-TNF nanomedicine. J clin Oncol. 2009; 27(15):3586.

Libutti SK, Paciotti GF, Byrnes AA, et al. Phase I and pharmacokinetic studies of CYT-6091, a novel PEGylated colloidal gold-rhTNF nanomedicine. Clin Cancer Res. 2010; 16(24):6139–6149.10.1158/1078-0432.ccr-10-0978 [PubMed: 20876255]

Lindhardt C, Schönenbrücher H, Slaghuis J, Bubert A, Ossmer R. Singlepath salmonella. Performance tested method 060401. J AOAC Int. 2009; 92(6):1885–1889. [PubMed: 20166612]

Link S, El-Sayed MA. Size and temperature dependence of the plasmon absorption of colloidal gold nanoparticles. J Phys Chem B. 1999; 103(21):4212–4217.10.1021/jp984796o

Link S, El-Sayed MA. Optical properties and ultrafast dynamics of metallic nanocrystals. Annu Rev Phys Chem. 2003; 54:331–366.10.1146/annurev.physchem.54.011002.103759 [PubMed: 12626731]

Liu Y, Huang CZ. Screening sensitive nanosensors via the investigation of shape-dependent localized surface plasmon resonance of single Ag nanoparticles. Nanoscale. 2013; 5(16):7458–7466.10.1039/c3nr01952g [PubMed: 23831964]

Liu X, Dai Q, Austin L, et al. A one-step homogeneous immunoassay for cancer biomarker detection using gold nanoparticle probes coupled with dynamic light scattering. J Am Chem Soc. 2008; 130(9):2780–2782.10.1021/ja711298b [PubMed: 18257576]

Liu X, Lee Py, Ho Cm, et al. Silver nanoparticles mediate differential responses in keratinocytes and fibroblasts during skin wound healing. ChemMedChem. 2010a; 5(3):468–475. [PubMed: 20112331]

Liu Z, Kiessling F, Gatjens J. Advanced nanomaterials in multimodal imaging: design, functionalization, and biomedical applications. J Nanomater. 2010b10.1155/2010/894303

Lu L, Sun RWY, Chen R, et al. Silver nanoparticles inhibit hepatitis B virus replication. Antiviral Ther. 2008; 13(2):253–262.

Lu W, Xiong C, Zhang G, et al. Targeted photothermal ablation of murine melanomas with melanocyte-stimulating hormone analog-conjugated hollow gold nanospheres. Clin Cancer Res. 2009a; 15(3):876–886.10.1158/1078-0432.ccR-08-1480 [PubMed: 19188158]

Lu X, Rycenga M, Skrabalak SE, Wiley B, Xia Y. Chemical synthesis of novel plasmonic nanoparticles. Annu Rev Phys Chem. 2009b; 60(1):167–192.10.1146/annurev.physchem.040808.090434 [PubMed: 18976140]

Lundqvist M, Stigler J, Elia G, Lynch I, Cedervall T, Dawson KA. Nanoparticle size and surface properties determine the protein corona with possible implications for biological impacts. Proc Natl Acad Sci USA. 2008; 105(38):14265–14270.10.1073/pnas.0805135105 [PubMed: 18809927]

Mackey MA, Saira F, Mahmoud MA, El-Sayed MA. Inducing cancer cell death by targeting its nucleus: solid gold nanospheres versus hollow gold nanocages. Bioconjugate Chem. 2013; 24(6):897–906.10.1021/bc300592d

Mackey MA, Ali MR, Austin LA, Near RD, El-Sayed MA. The most effective gold nanorod size for plasmonic photothermal therapy: theory and in vitro experiments. J Phys Chem B. 2014; 118(5): 1319–1326.10.1021/jp409298f [PubMed: 24433049]

Mahmoud MA, El-Sayed MA. Metallic double shell hollow nanocages: the challenges of their synthetic techniques. Langmuir. 2012; 28(9):4051–4059.10.1021/la203982h [PubMed: 22239672]

Mahmoud MA, El-Sayed MA. Different plasmon sensing behavior of silver and gold nanorods. J Phys Chem Lett. 2013; 4(9):1541–1545.10.1021/jz4005015

Mahmoud MA, El-Sayed MA, Gao J, Landman U. High-frequency mechanical stirring initiates anisotropic growth of seeds requisite for synthesis of asymmetric metallic nanoparticles like silver nanorods. Nano Lett. 2013; 13(10):4739–4745.10.1021/nl402305n [PubMed: 24053557]

Maiti KK, Samanta A, Vendrell M, Soh KS, Olivo M, Chang YT. Multiplex cancer cell detection by SERS nanotags with cyanine and triphenylmethine Raman reporters. Chem Commun. 2011; 47(12):3514–3516.10.1039/c0cc05265e

Maiti KK, Dinish US, Samanta A, et al. Multiplex targeted in vivo cancer detection using sensitive near-infrared SERS nanotags. Nano Today. 2012; 7(2):85–93.10.1016/j.nantod.2012.02.008

Mandecki, W.; Bharill, S.; Borejdo, J., et al. Fluorescence enhancement on silver nanostructures: studies of components of ribosomal translation in vitro—art. no. 68620T. In: Enderlein, J.; Gryczynski, ZK.; Erdmann, R., editors. Single molecule spectroscopy and imaging Proc Soc Photo Opt Instrum Eng. Vol. 6862. 2008. p. T8620-T8620.

Mao X, Ma YQ, Zhang AG, Zhang LR, Zeng LW, Liu GD. Disposable nucleic acid biosensors based on gold nanoparticle probes and lateral flow strip. Anal Chem. 2009; 81(4):1660–1668.10.1021/ac8024653 [PubMed: 19159221]

Marambio-Jones C, Hoek EMV. A review of the antibacterial effects of silver nanomaterials and potential implications for human health and the environment. J Nanopart Res. 2010; 12(5):1531–1551.10.1007/s11051-010-9900-y

Mark D, Haeberle S, Roth G, von Stetten F, Zengerle R. Microfluidic lab-on-a-chip platforms: requirements, characteristics and applications. Chem Soc Rev. 2010; 39(3):1153–1182.10.1039/b820557b [PubMed: 20179830]

McIntosh CM, Esposito EA, Boal AK, Simard JM, Martin CT, Rotello VM. Inhibition of DNA transcription using cationic mixed monolayer protected gold clusters. J Am Chem Soc. 2001; 123(31):7626–7629.10.1021/ja015556g [PubMed: 11480984]

Melancon MP, Lu W, Yang Z, et al. In vitro and in vivo targeting of hollow gold nanoshells directed at epidermal growth factor receptor for photothermal ablation therapy. Mol Cancer Ther. 2008; 7(6):1730–1739.10.1158/1535-7163.McT-08-0016 [PubMed: 18566244]

Mirkin CA, Letsinger RL, Mucic RC, Storhoff JJ. A DNA-based method for rationally assembling nanoparticles into macroscopic materials. Nature. 1996; 382(6592):607–609.10.1038/382607a0 [PubMed: 8757129]

Mohs A, Mancini M, Singhal S, et al. Hand-held spectroscopic device for in vivo and intraoperative tumor detection: contrast enhancement, detection sensitivity, and tissue penetration. Anal Chem. 2010; 82(21):9058–9065.10.1021/ac102058k [PubMed: 20925393]

Morones JR, Elechiguerra JL, Camacho A, et al. The bactericidal effect of silver nanoparticles. Nanotechnology. 2005; 16(10):2346. [PubMed: 20818017]

Mout R, Moyano DF, Rana S, Rotello VM. Surface functionalization of nanoparticles for nanomedicine. Chem Soc Rev. 2012; 41(7):2539–2544. [PubMed: 22310807]

Murphy CJ, Gole AM, Hunyadi SE, et al. Chemical sensing and imaging with metallic nanorods. Chem Commun. 2008; 5:544–557.10.1039/b711069c

Murthy SK. Nanoparticles in modern medicine: state of the art and future challenges. Int J Nanomed. 2007; 2(2):129.

Nath N, Chilkoti A. A colorimetric gold nanoparticle sensor to interrogate biomolecular interactions in real time on a surface. Anal Chem. 2001; 74(3):504–509.10.1021/ac015657x [PubMed: 11838667]

Nie SM, Emery SR. Probing single molecules and single nanoparticles by surface-enhanced Raman scattering. Science. 1997; 275(5303):1102–1106.10.1126/science.275.5303.1102 [PubMed: 9027306]

Nikoobakht B, El-Sayed MA. Preparation and growth mechanism of gold nanorods (NRs) using seed-mediated growth method. Chem Mater. 2003; 15(10):1957–1962.10.1021/cm020732l

Nolsoe CP, Torp-Pedersen S, Burcharth F, et al. Interstitial hyperthermia of colorectal liver metastases with a US-guided Nd-YAG laser with a diffuser tip: a pilot clinical study. Radiology. 1993; 187(2):333–337.10.1148/radiology.187.2.8475269 [PubMed: 8475269]

Nyamweya S, Hegedus A, Jaye A, Rowland-Jones S, Flanagan KL, Macallan DC. Comparing HIV-1 and HIV-2 infection: lessons for viral immunopathogenesis. Rev Med Virol. 2013; 23(4):221–240.10.1002/rmv.1739 [PubMed: 23444290]

Oishi M, Nakaogami J, Ishii T, Nagasaki Y. Smart PEGylated gold nanoparticles for the cytoplasmic delivery of siRNA to induce enhanced gene silencing. Chem Lett. 2006; 35(9):1046–1047.10.1246/cl.2006.1046

O'Neal DP, Hirsch LR, Halas NJ, Payne JD, West JL. Photo-thermal tumor ablation in mice using near infrared-absorbing nanoparticles. Cancer Lett. 2004; 209(2):171–176.10.1016/j.canlet.2004.02.004 [PubMed: 15159019]

Otto, A.; Futamata, M. Electronic mechanisms of SERS. In: Kneipp, K.; Moskovits, M.; Kneipp, H., editors. Surface-enhanced Raman Scattering: physics and applications Top Appl Phys. Vol. 103. 2006. p. 147-182.

Oyelere AK, Chen PC, Huang X, El-Sayed IH, El-Sayed MA. Peptide-conjugated gold nanorods for nuclear targeting. Bioconjugate Chem. 2007; 18(5):1490–1497.10.1021/bc070132i

Paciotti GF, Myer LD, Kim TH, et al. Colloidal gold: a novel colloidal nanoparticle vector for tumor-directed drug delivery. Clin Cancer Res. 2001; 7(11):3673S–3674S.

Paciotti GF, Myer L, Weinreich D, et al. Colloidal gold: a novel nanoparticle vector for tumor directed drug delivery. Drug Deliv. 2004; 11(3):169–183.10.1080/10717540490433895 [PubMed: 15204636]

Paciotti GF, Kingston DGI, Tamarkin L. Colloidal gold nanoparticles: a novel nanoparticle platform for developing multi-functional tumor-targeted drug delivery vectors. Drug Dev Res. 2006; 67(1):47–54.10.1002/Ddr.20066

Pal S, Tak YK, Song JM. Does the antibacterial activity of silver nanoparticles depend on the shape of the nanoparticle? A study of the gram-negative bacterium *Escherichia coli*. Appl Environ Microbiol. 2007; 73(6):1712–1720.10.1128/aem.02218-06 [PubMed: 17261510]

Park C, Kim H, Hixon D, Bubert A. Evaluation of the Duopath verotoxin test for detection of Shiga toxins in cultures of human stools. J Clin Microbiol. 2003; 41(6):2650–2653. [PubMed: 12791895]

Perrault SD, Chan WCW. Synthesis and surface modification of highly monodispersed, spherical gold nanoparticles of 50–200 nm. J Am Chem Soc. 2009; 131(47):17042–17043.10.1021/ja907069u [PubMed: 19891442]

Petryayeva E, Krull UJ. Localized surface plasmon resonance: nanostructures, bioassays and biosensing—a review. Anal Chim Acta. 2011; 706(1):8–24.10.1016/j.aca.2011.08.020 [PubMed: 21995909]

Pissuwan D, Niidome T, Cortie MB. The forthcoming applications of gold nanoparticles in drug and gene delivery systems. J Controlled Release. 2011; 149(1):65–71.10.1016/j.jconrel.2009.12.006

Pitsillides CM, Joe EK, Wei X, Anderson RR, Lin CP. Selective cell targeting with light-absorbing microparticles and nanoparticles. Biophys J. 2003; 84(6):4023–4032.10.1016/S0006-3495(03)75128-5 [PubMed: 12770906]

Prabaharan M, Grailer JJ, Pilla S, Steeber DA, Gong SQ. Gold nanoparticles with a monolayer of doxorubicin-conjugated amphiphilic block copolymer for tumor-targeted drug delivery. Biomaterials. 2009; 30(30):6065–6075.10.1016/j.biomaterials.2009.07.048 [PubMed: 19674777]

Pustovit VN, Shahbazyan TV. Resonance energy transfer near metal nanostructures mediated by surface plasmons. Phys Rev B Condens Matter Mater Phys. 2011; 83(8):085427.

Pyatenko A, Yamaguchi M, Suzuki M. Synthesis of spherical silver nanoparticles with controllable sizes in aqueous solutions. J Phys Chem C. 2007; 111(22):7910–7917.10.1021/jp071080x

Qian XM, Nie SM. Single-molecule and single-nanoparticle SERS: from fundamental mechanisms to biomedical applications. Chem Soc Rev. 2008; 37(5):912–920.10.1039/b708839f [PubMed: 18443676]

Qian XM, Peng XH, Ansari DO, et al. In vivo tumor targeting and spectroscopic detection with surface-enhanced Raman nanoparticle tags. Nat Biotechnol. 2008; 26(1):83–90.10.1038/nbt1377 [PubMed: 18157119]

Quang Huy T, van Quy N, Anh-Tuan L. Silver nanoparticles: synthesis, properties, toxicology, applications and perspectives. Adv Natl Sci Nanosci Nanotechnol. 2013; 4(3):033001.

Rai M, Yadav A, Gade A. Silver nanoparticles as a new generation of antimicrobials. Biotechnol Adv. 2009; 27(1):76–83.10.1016/j.biotechadv.2008.09.002 [PubMed: 18854209]

Ray PC, Fortner A, Darbha GK. Gold nanoparticle based FRET asssay for the detection of DNA cleavage. J Phys Chem B. 2006; 110(42):20745–20748.10.1021/jp0651211 [PubMed: 17048879]

Ray PC, Darbha GK, Ray A, Walker J, Hardy W. Gold nanoparticle based FRET for DNA detection. Plasmonics. 2007; 2(4):173–183.10.1007/s11468-007-9036-9

Richmond TD. The current status and future potential of personalized diagnostics: streamlining a customized process. Biotechnol Ann Rev. 2008; 14:411–422. [PubMed: 18606372]

Rong-Hwa S, Shiao-Shek T, Der-Jiang C, Yao-Wen H. Gold nanoparticle-based lateral flow assay for detection of staphylococcal enterotoxin B. Food Chem. 2010; 118(2):462–466.10.1016/j.foodchem.2009.04.106

Rosi NL, Giljohann DA, Thaxton CS, Lytton-Jean AKR, Han MS, Mirkin CA. Oligonucleotide-modified gold nanoparticles for intracellular gene regulation. Science. 2006; 312(5776):1027–1030.10.1126/science.1125559 [PubMed: 16709779]

Sapsford KE, Algar WR, Berti L, et al. Functionalizing nanoparticles with biological molecules: developing chemistries that facilitate nanotechnology. Chem Rev. 2013; 113(3):1904–2074.10.1021/cr300143v [PubMed: 23432378]

Schatz GC, Young MA, Van Duyne RP. Electromagnetic mechanism of SERS. Surfac enhanc Raman Scatt Phys Appl. 2006; 103:19–45.

Schlücker S. SERS microscopy: nanoparticle probes and biomedical applications. ChemPhysChem. 2009; 10(9–10):1344–1354.10.1002/cphc.200900119 [PubMed: 19565576]

Schmidt M, Hübner J, Boisen A. Large area fabrication of leaning silicon nanopillars for surface enhanced Raman spectroscopy. Adv Mater. 2012; 24(10):8.10.1002/adma.201103496

Seferos D, Giljohann D, Hill H, Prigodich A, Mirkin C. Nano-flares: probes for transfection and mRNA detection in living cells. J Am Chem Soc. 2007; 129(50):15477–15479.10.1021/ja0776529 [PubMed: 18034495]

Sershen SR, Westcott SL, Halas NJ, West JL. Temperature-sensitive polymer-nanoshell composites for photothermally modulated drug delivery. J Biomed Mater Res. 2000; 51(3):293–298.10.1002/1097-4636(20000905)51:3<293:AidJbm1>3.0.co;2-T [PubMed: 10880069]

Sharma VK, Yngard RA, Lin Y. Silver nanoparticles: green synthesis and their antimicrobial activities. Adv Colloid Interf Sci. 2009; 145(1–2):83–96.10.1016/j.cis.2008.09.002

Sharma B, Ma K, Glucksberg MR, Van Duyne RP. Seeing through bone with surface-enhanced spatially offset Raman spectroscopy. J Am Chem Soc. 2013; 135(46):17290–17293.10.1021/ja409378f [PubMed: 24199792]

Sherry LJ, Chang SH, Schatz GC, Van Duyne RP, Wiley BJ, Xia Y. Localized surface plasmon resonance spectroscopy of single silver nanocubes. Nano Lett. 2005; 5(10):2034–2038.10.1021/nl0515753 [PubMed: 16218733]

Shiotani A, Akiyama Y, Kawano T, et al. Active accumulation of gold nanorods in tumor in response to near-infrared laser irradiation. Bioconjugate Chem. 2010; 21(11):2049–2054.10.1021/bc100284s

Skrabalak SE, Chen J, Sun Y, et al. Gold nanocages: synthesis, properties, and applications. Acc Chem Res. 2008; 41(12):1587–1595.10.1021/ar800018v [PubMed: 18570442]

Sondi I, Salopek-Sondi B. Silver nanoparticles as antimicrobial agent: a case study on *E-coli* as a model for Gram-negative bacteria. J Colloid Interf Sci. 2004; 275(1):177–182.10.1016/j.jcis.2004.02.012

Sperling R, Parak W. Surface modification, functionalization and bioconjugation of colloidal inorganic nanoparticles. Philos Trans R Soc A Math Phys Eng Sci. 2010; 368(1915):1333–1383.

Sriram MI, Kanth SBM, Kalishwaralal K, Gurunathan S. Anti-tumor activity of silver nanoparticles in Dalton's lymphoma ascites tumor model. Int J Nanomed. 2010; 5:753.

Storhoff JJ, Elghanian R, Mucic RC, Mirkin CA, Letsinger RL. One-pot colorimetric differentiation of polynucleotides with single base imperfections using gold nanoparticle probes. J Am Chem Soc. 1998; 120(9):1959–1964.10.1021/ja972332i

Sun Y, Xia Y. Shape-controlled synthesis of gold and silver nanoparticles. Science. 2002; 298(5601): 2176–2179.10.1126/science.1077229 [PubMed: 12481134]

Sun L, Yu C, Irudayaraj J. Surface-enhanced Raman scattering based nonfluorescent probe for multiplex DNA detection. Anal Chem. 2007; 79(11):3981–3988.10.1021/ac070078z [PubMed: 17465531]

Swathi RS, Sebastian KL. Resonance energy transfer from a fluorescent dye molecule to plasmon and electron-hole excitations of a metal nanoparticle. J Chem Phys. 2007; 126(23):234701. [PubMed: 17600429]

Tao AR, Habas S, Yang PD. Shape control of colloidal metal nanocrystals. Small. 2008; 4(3):310–325.10.1002/smll.200701295

Tao H, Liao X, Xu M, Xie X, Zhong F, Yi Z. Detection of immunoglobulin G based on nanoparticle surface energy transfers from fluorescein isothiocyanate to gold nanoparticles. Anal Methods. 201410.1039/c3ay41957f

Tashkhourian J, Hormozi-Nezhad MR, Khodaveisi J, Dashti R. A novel photometric glucose biosensor based on decolorizing of silver nanoparticles. Sens Actuators, B. 2011; 158(1):185–189.10.1016/j.snb.2011.06.002

Tian J, wong KK, Ho CM, et al. Topical delivery of silver nanoparticles promotes wound healing. ChemMedChem. 2007; 2(1):129–136. [PubMed: 17075952]

Ting BP, Zhang J, Gao ZQ, Ying JY. A DNA biosensor based on the detection of doxorubicin-conjugated Ag nanoparticle labels using solid-state voltammetry. Biosens Bioelectron. 2009; 25(2):282–287.10.1016/j.bios.2009.07.005 [PubMed: 19665881]

Tippkotter N, Stuckmann H, Kroll S, et al. A semi-quantitative dipstick assay for microcystin. Anal Bioanal Chem. 2009; 394(3):863–869.10.1007/s00216-009-2750-8 [PubMed: 19306114]

Tocco I, Zavan B, Bassetto F, Vindigni V. Nanotechnology-based therapies for skin wound regeneration. J Nanomater. 201210.1155/2012/714134

Tripp RA, Dluhy RA, Zhao Y. Novel nanostructures for SERS biosensing. Nano Today. 2008; 3(3): 31–37.

Turkevich J, Stevenson PC, Hillier J. A study of the nucleation and growth processes in the synthesis of colloidal gold. Discuss Faraday Soc. 1951; 11:55–75.10.1039/df9511100055

Van de Broek B, Devoogdt N, D'Hollander A, et al. Specific cell targeting with nanobody conjugated branched gold nanoparticles for photothermal therapy. ACS Nano. 2011; 5(6):4319–4328.10.1021/Nn1023363 [PubMed: 21609027]

Vigderman L, Zubarev ER. Therapeutic platforms based on gold nanoparticles and their covalent conjugates with drug molecules. Adv Drug Delivery Rev. 2013; 65(5):663–676.

Vo-Dinh T, Wang HN, Scaffidi J. Plasmonic nanoprobes for SERS biosensing and bioimaging. J Biophotonics. 2010; 3(1–2):89–102.10.1002/jbio.200910015 [PubMed: 19517422]

Wang C, Irudayaraj J. Gold nanorod probes for the detection of multiple pathogens. Small. 2008; 4(12):2204–2208.10.1002/smll.200800309 [PubMed: 19003819]

Wang F, Wang YC, Dou S, Xiong MH, Sun TM, Wang J. Doxorubicin-tethered responsive gold nanoparticles facilitate intracellular drug delivery for overcoming multidrug resistance in cancer cells. ACS Nano. 2011a; 5(5):3679–3692.10.1021/Nn200007z [PubMed: 21462992]

Wang J, Byrne JD, Napier ME, DeSimone JM. More effective nanomedicines through particle design. Small. 2011b; 7(14):1919–1931.10.1002/smll.201100442 [PubMed: 21695781]

Wang Y, Tang LJ, Jiang JH. Surface-enhanced raman spectroscopy-based, homogeneous, multiplexed immunoassay with antibody-fragments-decorated gold nanoparticles. Anal Chem. 2013; 85(19): 9213–9220.10.1021/ac4019439 [PubMed: 23998432]

Wei H, Chen CG, Han BY, Wang EK. Enzyme colorimetric assay using unmodified silver nanoparticles. Anal Chem. 2008; 80(18):7051–7055.10.1021/ac801144t [PubMed: 18662017]

Weissleder R. A clearer vision for in vivo imaging. Nat Biotechnol. 2001; 19(4):316–317.10.1038/86684 [PubMed: 11283581]

Wiethoff CM, Middaugh CR. Barriers to nonviral gene delivery. J Pharm Sci. 2003; 92(2):203–217.10.1002/Jps.10286 [PubMed: 12532370]

Willets KA, Van Duyne RP. Localized surface plasmon resonance spectroscopy and sensing. Annu Rev Phys Chem. 2007; 58(1):267–297.10.1146/annurev.physchem.58.032806.104607 [PubMed: 17067281]

Xiang DX, Chen Q, Pang L, Zheng CL. Inhibitory effects of silver nanoparticles on H1N1 influenza A virus in vitro. J Virol Methods. 2011; 178(1–2):137–142.10.1016/j.jviromet.2011.09.003 [PubMed: 21945220]

Xu X, Chen Y, Wei HJ, Xia B, Liu F, Li N. Counting bacteria using functionalized gold nanoparticles as the light-scattering reporter. Anal Chem. 2012; 84(22):9721–9728.10.1021/ac302471c [PubMed: 23035847]

Yu AK, Kudrinskiy AA, Olenin AY, Lisichkin GV. Synthesis and properties of silver nanoparticles: advances and prospects. Russ Chem Rev. 2008; 77(3):233.

Yuan Y, Zhang J, Zhang H, Yang X. Silver nanoparticle based label-free colorimetric immunosensor for rapid detection of neurogenin 1. Analyst. 2012; 137(2):496–501.10.1039/c1an15875a [PubMed: 22114758]

Yun CS, Javier A, Jennings T, et al. Nanometal surface energy transfer in optical rulers, breaking the FRET barrier. J Am Chem Soc. 2005; 127(9):3115–3119.10.1021/ja043940i [PubMed: 15740151]

Zavaleta CL, Smith BR, walton I, et al. Multiplexed imaging of surface enhanced Raman scattering nanotags in living mice using noninvasive Raman spectroscopy. Proc Natl Acad Sci. 2009; 106(32):13511–13516.10.1073/pnas.0813327106 [PubMed: 19666578]

Zhu K, Zhang Y, He S, et al. Quantification of proteins by functionalized gold nanoparticles using click chemistry. Anal Chem. 2012; 84(10):4267–4270.10.1021/ac3010567 [PubMed: 22540271]

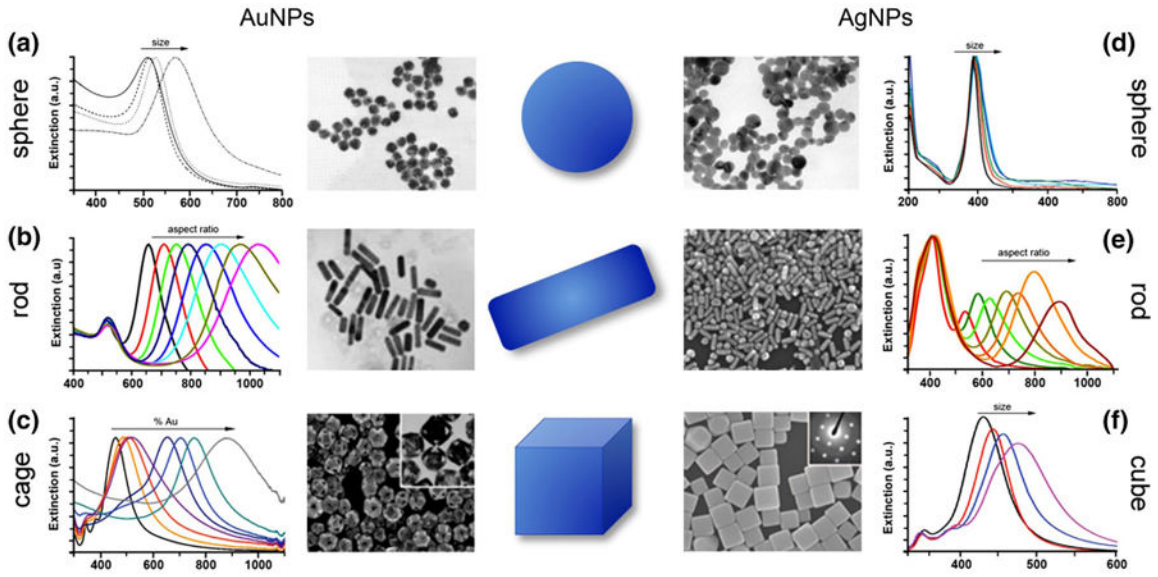

Fig. 1.

Commonly synthesized Au and Ag nanostructures for biodiagnostic and therapeutic applications. Graphical illustrations, electron micrographs, and extinction spectra for **a** Au nanospheres, **b** Au nanorods, **c** Au nanocages, **d** Ag nanospheres, **e** Ag nanorods, and **f** Ag nanocubes. *Observed red-shift* in extinction spectra is representative of increasing nanostructure size (**a**, **d**, **f**), increasing aspect ratio (**b**, **e**), and increasing gold deposition (**c**). Reprinted with permission from **a** (Link and El-Sayed 1999), **b** (Huang et al. 2009), **c** (Skrabalak et al. 2008) and (Chen et al. 2006), **d** (Pyatenko et al. 2007), **e** (Mahmoud and El-Sayed 2013), and **f** (Mahmoud and El-Sayed 2012) and (Chen et al. 2006). Copyright. 1999 American Chemical Society, 2009 Wiley–VCH Verlag GmbH & Co. KGaA, 2008 American Chemical Society, 2006 American Chemical Society, 2007 American Chemical Society, 2013 American Chemical Society, 2012 American Chemical Society, and 2006 American Chemical Society, respectively

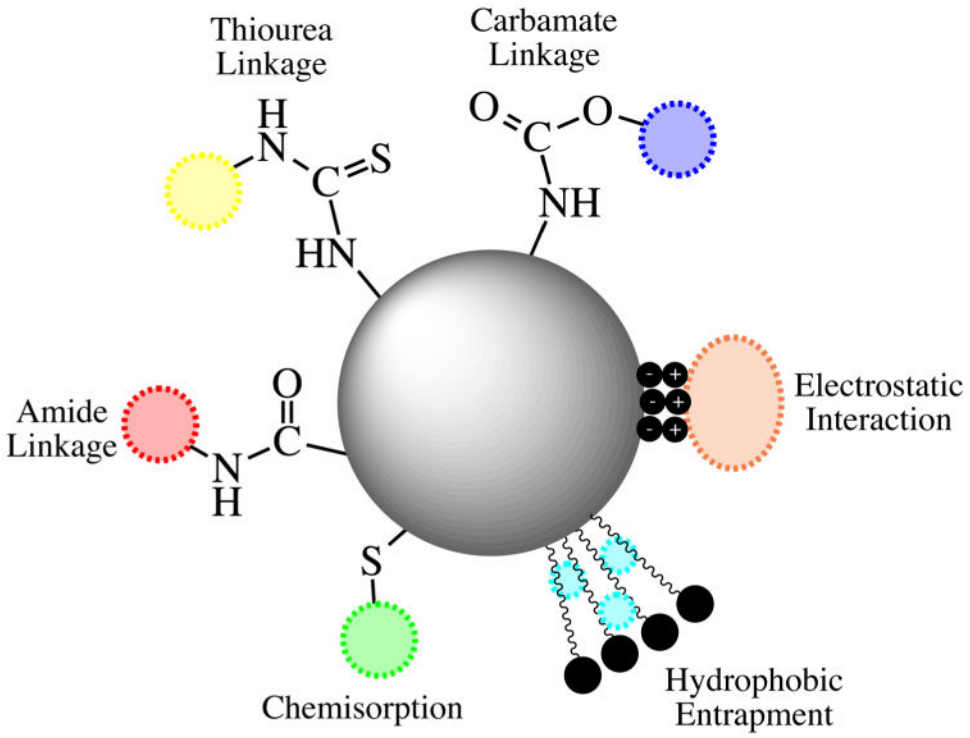

Fig. 2. Common functionalization strategies for Au and Ag nanostructures for use in biomedical applications

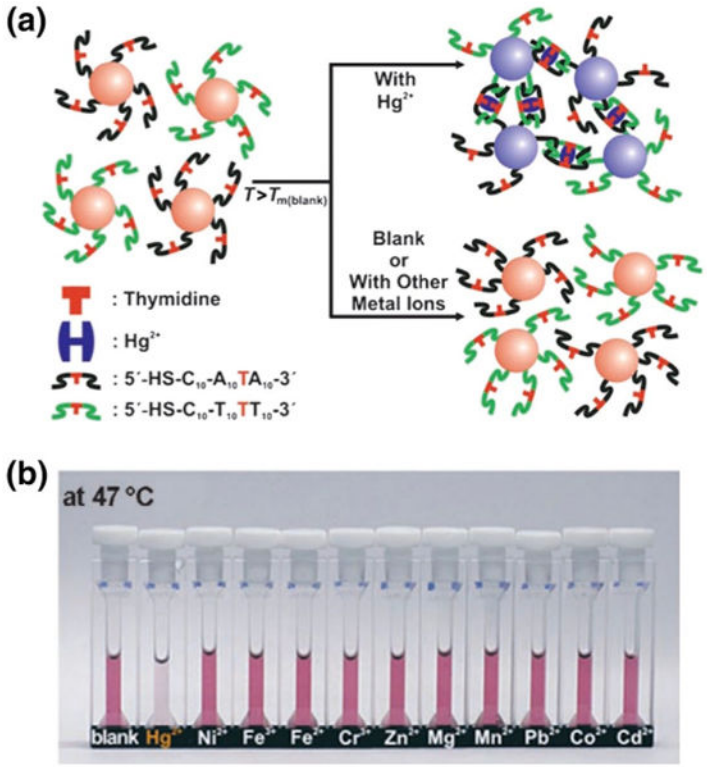

Fig. 3.

Colorimetric detection of mercuric ion using DNA-AuNPs. **a** Schematic diagram of the colorimetric Hg^{2+} assay. AuNPs were divided into two groups and functionalized with complementary DNA that contains a thymidine–thymidine mismatch as indicated in *red*. In the presence of Hg^{2+}, the DNA-AuNPs will form aggregates due to Hg^{2+} coordination at the T–T mismatch site. **b** The presence and concentration of Hg^{2+} ions can be determined by the color change (or LSPR shift) of the solution at a given temperatures. Reprinted with permission from (Lee et al. 2007). Copyright. 2007 Wiley–VCH Verlag GmbH & Co. KGaA

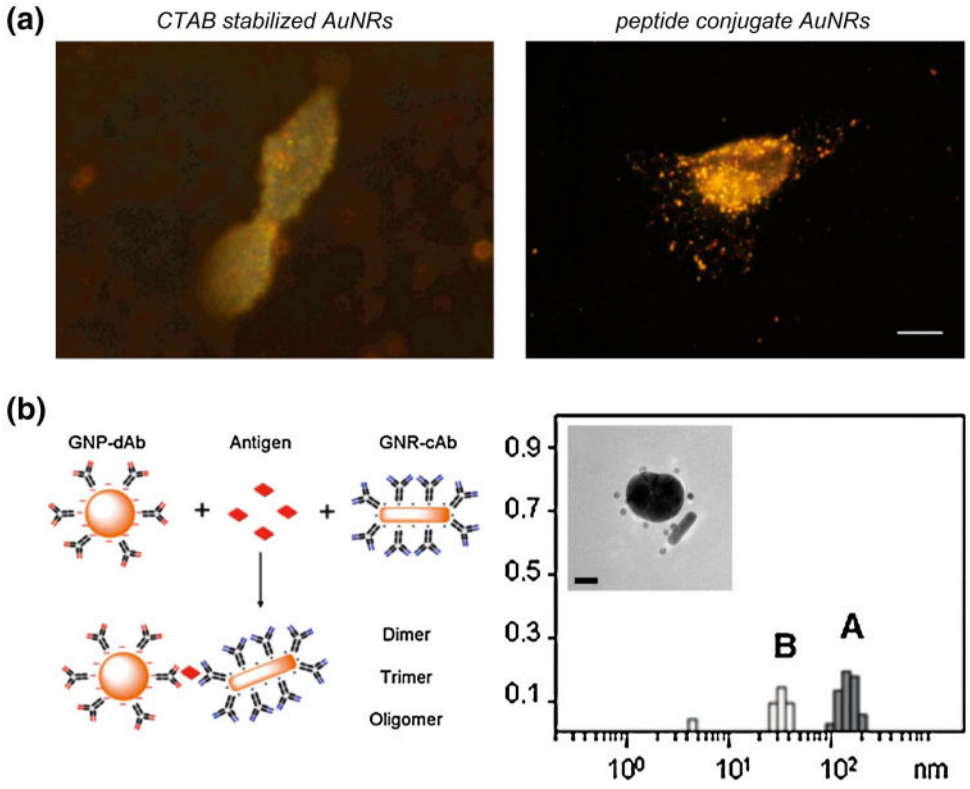

Fig. 4.

Surface-enhanced Rayleigh scattering applications of AuNPs. **a** Dark field light scattering was utilized to assess AuNR (*left*) and peptide-conjugated AuNR (*right*) uptake. Peptide conjugation determined to promote AuNR cellular uptake. *Scale bar* 10 μM. (**b**) Schematic diagram of fPSA detection using antibody-conjugated AuNSs and AuNRs (*left*). Nanoparticle incubation with fPSA caused two hydrodynamic diameter populations correlating to oligomer formation (*right A* and *inset*) and individual particles (*right B*). The peak area ratio between population A and population B reveals fPSA concentrations. **a** Reprinted with permission from (Oyelere et al. 2007). Copyright. 2007 American Chemical Society. **b** Reprinted with permission from (Liu et al. 2008). Copyright. 2008 American Chemical Society

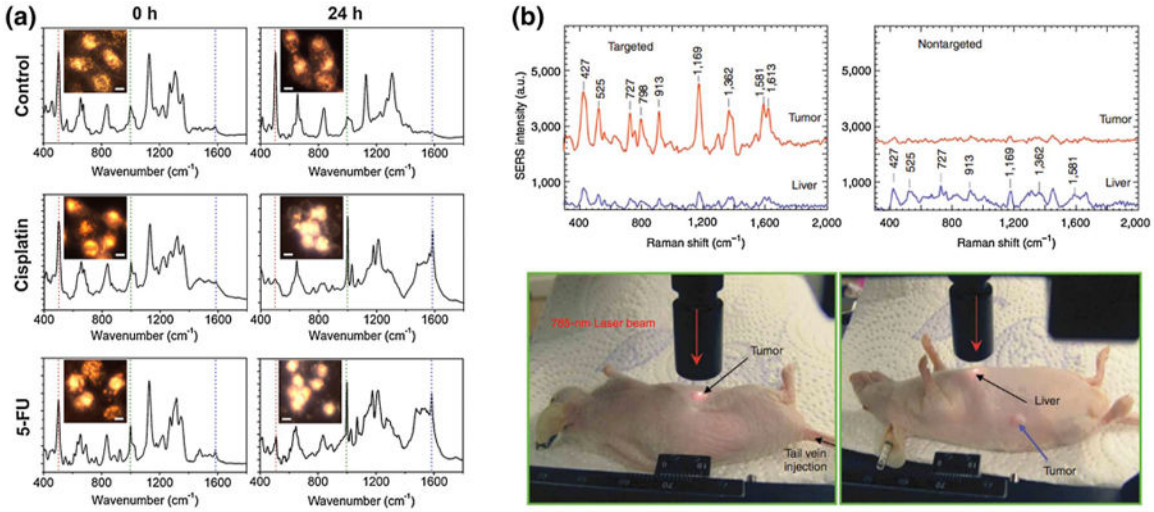

Fig. 5.

Surface-enhanced Raman scattering applications of AuNPs. **a** Live cell Rayleigh images and SERS spectra of cancer cells untreated (*top*) or treated with 100 M cisplatin (*middle*) or 5-FU (*bottom*). Apoptotic cell death and drug efficacy were determined by the increase or decrease in 500, 1,000, and 1,585 cm^{-1} band intensities. **b** In vivo SERS spectra obtained from tumor-targeted (*top left*) and nontargeted (*top right*) AuNPs. Raman reporter spectral signatures were observed in tumors of nude mice (*bottom left*) treated with tumor-targeting (ScFv antibody-conjugated) AuNPs, while nontargeted AuNPs showed Raman signal at the liver. **a** Reprinted with permission from (Austin et al. 2013). Copyright. 2013 American Chemical Society. **b** Reprinted with permission from (Qian et al. 2008). Copyright. 2008 Nature Publishing Group

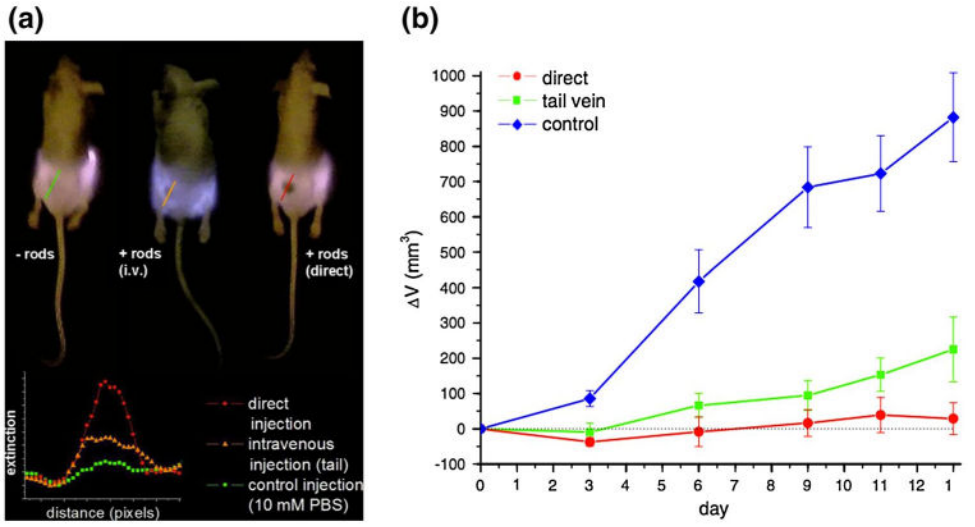

Fig. 6.

Plasmonic photothermal therapy (PPTT) using gold nanoparticles. **a** PEGylated gold nanorods accumulate in the tumor after both intravenous (+rods i.v.) and direct (+rods direct) injections as shown by the NIR transmission images (*top*) and increased NIR extinction (*bottom*) for intravenous (*orange*) and direct (*red*) injections compared with that of untreated tumors (*green*). **b** exposure of tumors, post-intravenous (*green*) and direct (*red*) injection of PEGylated gold nanorods, with cw NIR irradiation for 10 min causes a dramatic reduction in tumor volume over 13 days compared with untreated tumors (*blue*). Reprinted with permission from (Dickerson et al. 2008). Copyright 2008, Elsevier Ltd

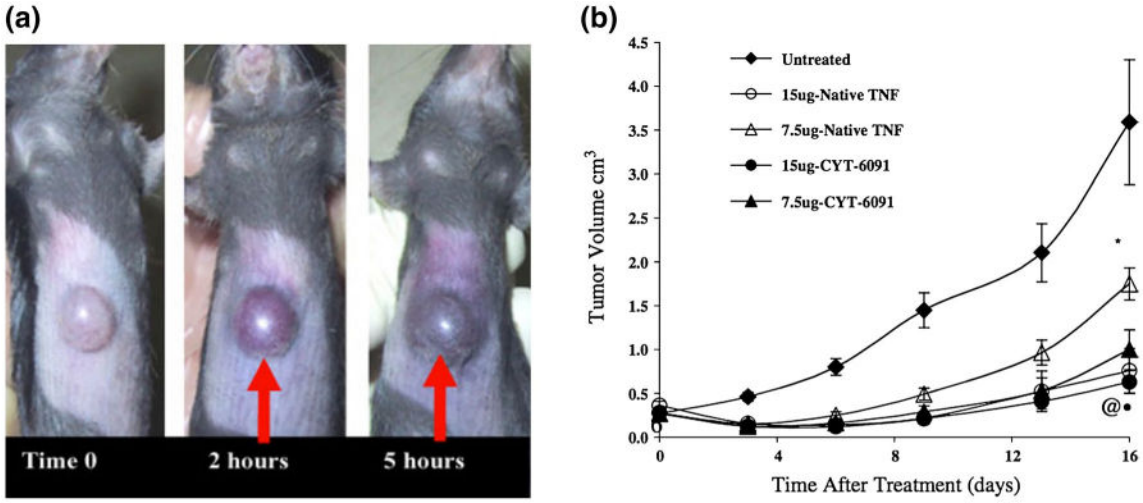

Fig. 7.

Targeted gold nanoparticles for drug delivery. **a** Spherical gold nanoparticles conjugated with tumor necrosis factor (TNF) effectively accumulate in tumors within 5 h. **b** CYT-6091 (TNF-conjugated gold nanoparticles) demonstrates similar antitumor efficacy as that of native TNF at high treatment concentrations of 15 μg, but with greater overall survival, indicating reduced toxicity with the nanoparticle drug formulation. At lower treatment concentrations (7.5 μg), CYT-6091 exhibits enhanced antitumor efficacy compared with the same concentration of native TNF. Reprinted with permission from (Paciotti et al. 2006). Copyright 2006, Wiley-Liss, Inc

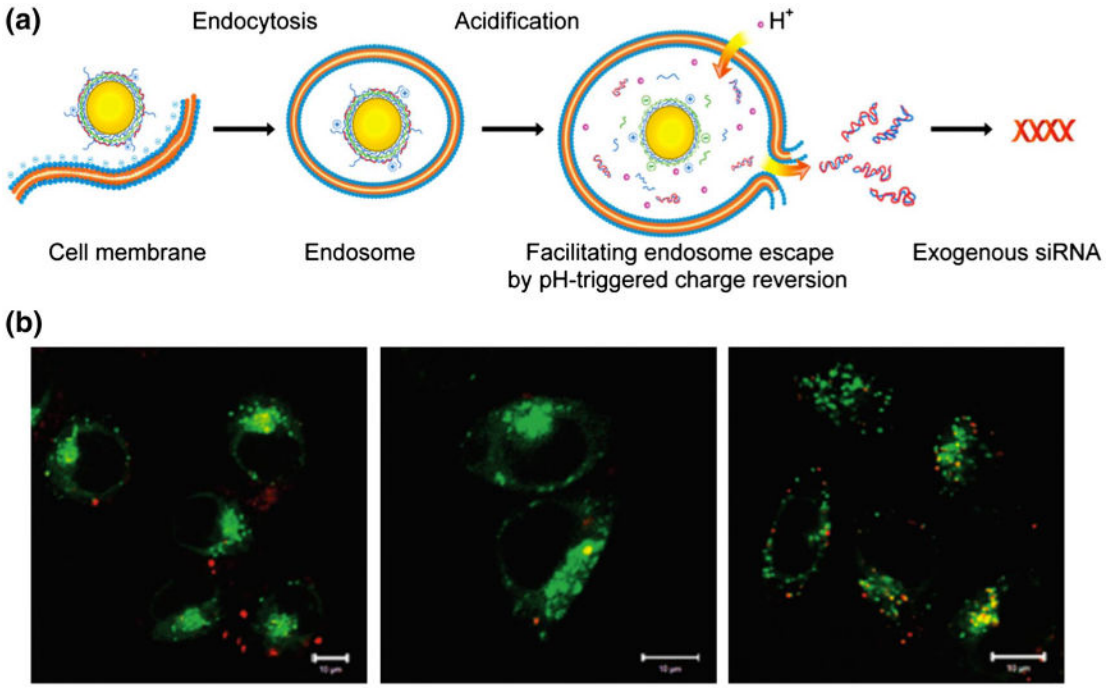

Fig. 8.

Charge-reversal polymer-coated gold nanoparticles for gene therapy. **a** The gold nanoparticle layer-by-layer coated with a charge-reversal polyelectrolyte and siRNA enters the cell through the endosome, upon which, the low pH reverses the charge of the polyelectrolyte allowing endosomal escape of siRNA into the cytoplasm. **b** confocal images of Hela cells stained with an endosome/lysosome stain (*green*) were taken after transfection with cy5-labeled siRNA (*red*) in the nanoparticle formulation (*left panel*), and in formulation with common transfection agents lipofectamine 2000 (*middle panel*) and PEI (*right panel*). The gold nanoparticle formulation of siRNA shows the presence of siRNA outside of the endosome/lysosome, while the transfection agent formulations of siRNA show colocalization of siRNA with the endosome/lysosome, indicating the gold nanoparticle formulation of siRNA is more effective in gene delivery than the common transfection agents currently in use. Reprinted with permission from (Guo et al. 2010). Copyright 2010, American Chemical Society

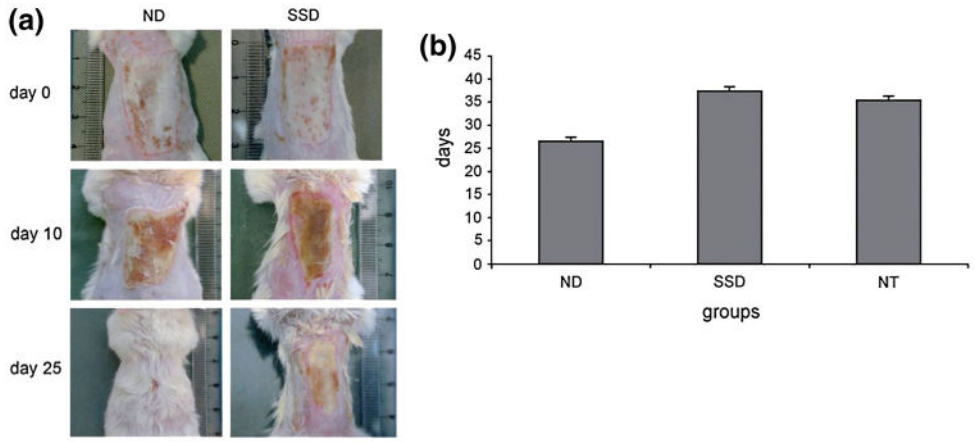

Fig. 9.

Topical administration of AgNPs promotes wound healing. **a** Photographic images of mice treated with 0.4777 mg of AgNPs (*left*) and 0.1502 g of silver sulfadiazine (*right*) at 0, 10, and 15 days indicate AgNP treatment led to accelerated wound healing and improved cosmetic outcomes. **b** Mice treated with AgNPs required ∼ 9 less days for burn wound healing compared to those treated with silver sulfadiazine and those administered no treatment. (*ND* AgNPs, *SSD* silver sulfadiazine, *NT* no treatment). Reprinted with permission from (Tian et al. 2007). Copyright 2007 Wiley–VCH Verlag GmbH & Co. KGaA

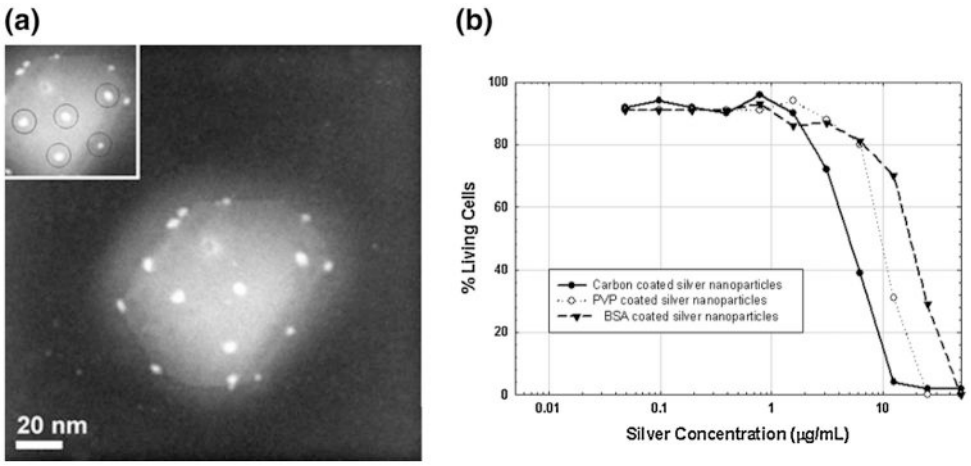

Fig. 10.

AgNP interaction on HIV-1 inhibits binding to host cells. **a** BSA-conjugated AgNPs, with diameters of 1–10 nm, interact with the HIV-1 virus in a distinct spatial arrangement suggesting AgNPs preferentially bind to gp120 glycoprotein knobs. **b** HIV-1 inhibition occurs in a dose-dependent manner and impacted by the degree of encapsulation by the AgNP capping agent. Reprinted with permission from (Elechiguerra et al. 2005). Copyright 2005 BioMed Central

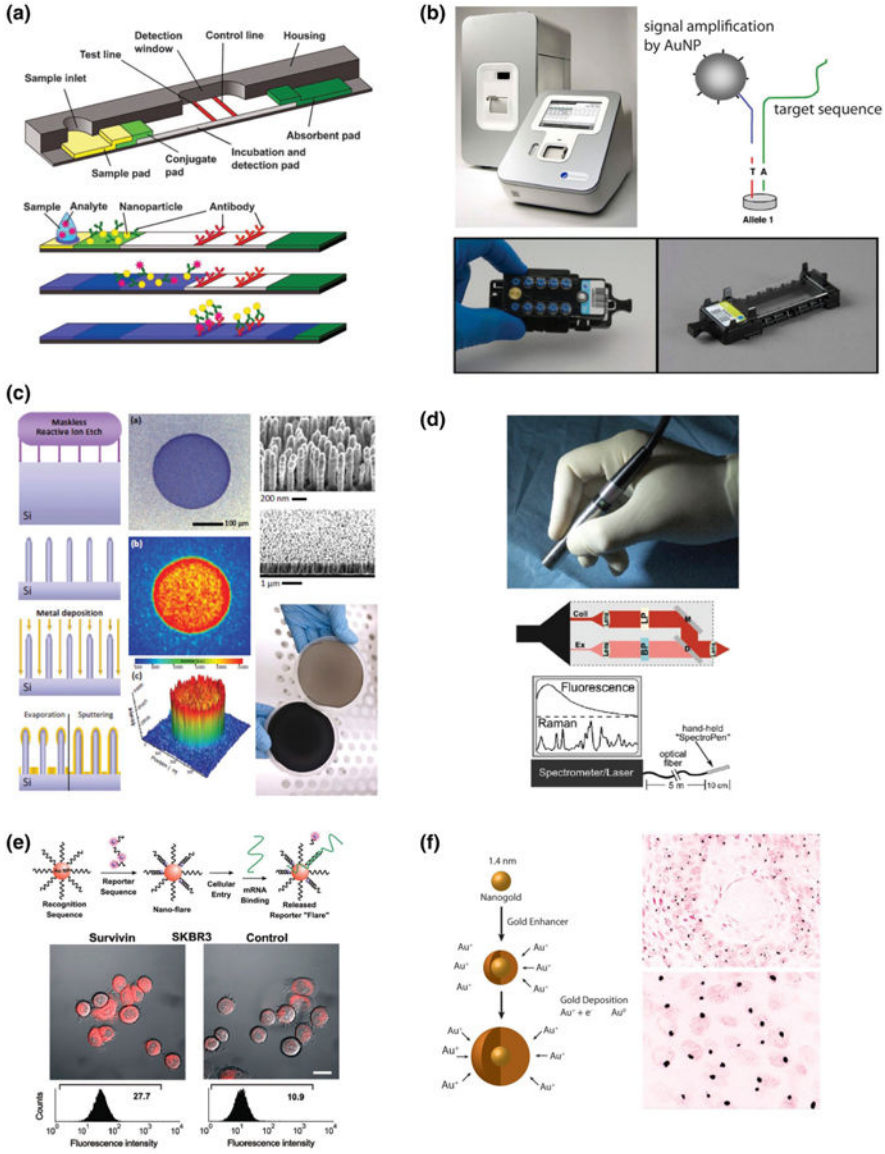

Fig. 11.

Applications of gold and silver nanotechnologies in clinical diagnostics. **a** Generalized schematic of a lateral flow assay (i.e., dipstick assay) that uses green light absorption by AuNPs to indicate the presence of antigen in complex biological fluids (e.g., the First Response™ pregnancy exam, Duopath™ verotoxin test, or ImmunoCAP™ allergy exam). **b** light scattering based nucleic acid and protein detection using the oligonucleotide-AuNP-based verigene™ detection system. **c** Substrates for reproducible enhancement of spectroscopic Raman scattering detection using Au- and Ag-coated SERStrate™ silicon nanopillar arrays. Fabrication (*left*), liquid droplet-induced generation of a homogenous spectroscopic hotspot (*middle*), and wafer-scale fabrication with and without Ag deposition (*right*). **d** Preclinical surgical guidance using AuNP-enhanced Raman scattering probes and a Spectropen™ handheld spectroscopic imaging device. **e** SmartFlare™ probes for live cell imaging of mRNA expression based on AuNP quenching of fluorophore-bound

oligonucleotides. **f** Detection of low virus copy HPV16/18 infection in a cervical squamous cell carcinoma histology section using streptavidin–gold nanoparticle conjugates. **a** Reprinted with permission from (Mark et al. 2010). copyright 2010 Royal Society of chemistry. **b** Reprinted with permission from (Lefferts et al. 2009). Copyright 2009 Elsevier Inc. **c** Reprinted with permission from (Schmidt et al. 2012). Copyright 2012 Wiley–VCH Verlag GmbH & Co. **d** Reprinted with permission from (Mohs et al. 2010). Copyright 2010 American Chemical Society. **e** Reprinted with permission from (Seferos et al. 2007). Copyright 2007 American Chemical Society. **f** Reprinted with permission from (Graf et al. 2000). Copyright 2000 Lippincott Williams & Wilkins

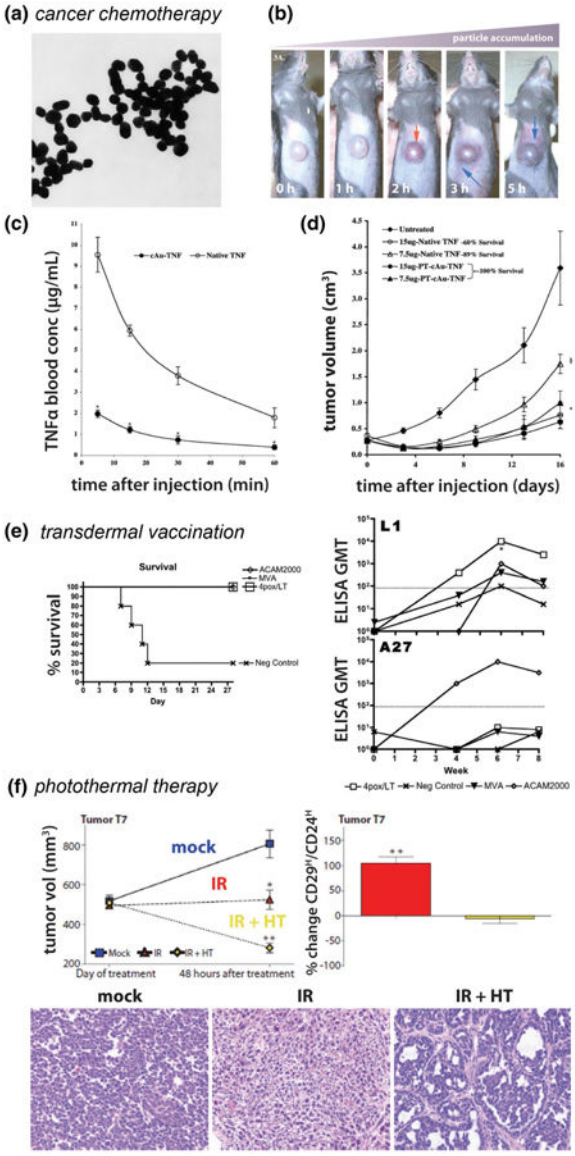

Fig. 12.

Applications of gold and silver nanotechnologies in clinical therapy. Tumor-targeted TNFα delivery using PEGylated **a** gold nanoparticles. **b** Aurimune™ accumulates in MC-38 tumor-bearing c57/BL6 mice over time with **c** improved circulation half-life and **d** AuNP-augmented tumor regression/survival. **e** Transdermal vaccination of nonhuman primates against monkeypox virus using gold nanoparticle vectors, DNA vaccine, and the handheld ND10 transdermal delivery device. Improved survival (*left*) and corresponding increases in antigen-specific antibodies in sera from nonhuman primates (*right*). **f** combined laser photothermal therapy (HT) and radiation therapy (IR) using PEGylated gold nanoshells reduces tumor burden (*top left*, *bottom*), decreases tumorigenicity, and induces more differentiated phenotype (*top right*) in murine models of breast carcinoma. **a**–**d** Reproduced with permission from (Paciotti et al. 2004). copyright 2004 Taylor & Francis Inc. **f**

reproduced with permission from (Atkinson et al. 2010). Copyright 2010 American Association for the Advancement of Science

Table 1

A compilation of reviews related to Au and Ag nanostructures for biomedical applications

Application	References
Synthesis	Grzelczak et al. (2008), Lu et al. (2009b), Quang Huy et al. (2013), Tao et al. (2008), Yu et al. (2008)
Biofunctionalization	Ju et al. (2011), Mout et al. (2012), Sapsford et al. (2013), Sperling and Parak (2010)
Localized surface plasmon resonance (LSPR) shift	Petryayeva and Krull (2011), Willets and Van Duyne (2007)
Enhanced rayleigh scattering	Jain et al. (2007), Li et al. (2012), Murphy et al. (2008)
Surface-enhanced Raman scattering (SeRS)	Jain et al. (2008), Kneipp et al. (2010), Qian and Nie (2008), Schlücker (2009), Tripp et al. (2008), Vo-Dinh et al. (2010)
Metal-enhanced fluorescence	Aslan et al. (2005), Lakowicz (2006)
Nanoparticle surface energy transfer (NSET)	Chen et al. (2013), Höppener and Novotny (2012)
Plasmonic photothermal therapy (PPTT)	Dreaden et al. (2011), Huang et al. (2008), Jain et al. (2008)
Drug Delivery	Dreaden et al. (2011), Ghosh et al. (2008), Kumar et al. (2013), Pissuwan et al. (2011), Vigderman and Zubarev (2013)
Gene therapy	Boisselier and Astruc (2009), Dreaden et al. (2011), Ghosh et al. (2008), Jeong et al. (2014), Pissuwan et al. (2011), Vigderman and Zubarev (2013)
Antimicrobial	Rai et al. (2009), Sharma et al. (2009), Vigderman and Zubarev (2013)
Wound Healing	Tocco et al. (2012)
Antiviral	Arvizo et al. (2012), Galdiero et al. (2011), Sharma et al. (2009)
Angiogenesis therapy	Arvizo et al. (2012), Boisselier and Astruc (2009), Dreaden et al. (2011)

It should be noted that this is not a comprehensive list